AGU PUBLICATIONS

JGR

Journal of Geophysical Research: Space Physics

RESEARCH ARTICLE

10.1002/2014JA019771

**Key Points:**
- Effect of preceding ICMEs on SEP transport influences SEP peak event intensities
- We provide upper limits of SEP peak intensities once CME speeds are known
- Results on preconditioning by preceding CMEs revised with low intensity events

**Correspondence to:**
D. Lario,
David.Lario@jhuapl.edu

**Citation:**
Lario, D., and A. Karelitz (2014), Influence of interplanetary coronal mass ejections on the peak intensity of solar energetic particle events, *J. Geophys. Res. Space Physics*, *119*, 4185–4209, doi:10.1002/2014JA019771.

Received 7 JAN 2014
Accepted 25 MAY 2014
Accepted article online 29 MAY 2014
Published online 24 JUN 2014

# Influence of interplanetary coronal mass ejections on the peak intensity of solar energetic particle events

**D. Lario[1] and A. Karelitz[2]**

[1]Applied Physics Laboratory, Johns Hopkins University, Laurel, Maryland, USA, [2]National Institute of Aerospace, Hampton, Virginia, USA

**Abstract** We study whether the presence of coronal mass ejections (CMEs) in interplanetary space (ICMEs) affects the maximum intensity of solar energetic particle (SEP) events. We compute the maximum intensity of 175–315 keV electron and 9–15, 15–40, and 40–80 MeV proton fluxes measured during the prompt component of 147 western SEP events observed near Earth throughout solar cycle 23. When using in situ observations to determine the presence and location of preceding ICMEs during SEP events, we find that, over the ensemble of events, those observed either within a preceding ICME or when a preceding ICME is beyond the observer's location have, on average, larger peak intensities than the events observed in absence of ICMEs. The few events observed when an Earth-directed ICME is located between the Sun and the observer tend to have lower 9–15 and 15–40 MeV proton peak intensities than the events without preceding ICMEs; the differences are not significant for 175–315 keV electron peak intensities. When using coronagraph observations to determine the presence of preceding CMEs, we find that, over the ensemble of events, those events (Case P) occurring within 24 h after the launch of a CME from the same active region as the primary CME generating the SEP event tend to have higher peak intensities than those events (Case NP) occurring without a preceding CME. The differences between the average peak intensities of these two event cases (P and NP) are smaller when we exclude events observed when a prior ICME is already located at or beyond Earth.

## 1. Introduction

Several factors control the variability of intensities measured in solar energetic particle (SEP) events [e.g., *Kahler et al.*, 1999; *Gopalswamy*, 2012]. Among them, the longitude of the parent solar event generating the SEP event [e.g., *Cane et al.*, 1988; *Lario et al.*, 2006] and the speed of the parent coronal mass ejection (CME) associated with the origin of the SEP event [e.g., *Reames*, 2000] are the dominant parameters controlling the peak intensity of the SEP events. Other factors suggested to play a role in the intensity of SEP events include the ambient (or preevent) SEP intensities [e.g., *Kahler et al.*, 1999; *Kahler*, 2001; *Gopalswamy et al.*, 2003], the presence of a preceding CME able to precondition the plasma where the main CME associated with the origin of the SEP event propagates [*Gopalswamy et al.*, 2004; *Li et al.*, 2012], the Alfvén speed distribution in the ambient medium where the parent or primary CME starts propagating [*Gopalswamy et al.*, 2008a], and the presence of coronal holes near the active region that generates the SEP event [*Gopalswamy*, 2012] (see also *Kahler et al.*, [2012, 2014] for a negative result on the possible effects that coronal holes have on SEP properties).

In this article, we study whether the medium through which SEPs propagate has a significant effect on the measured SEP peak intensities. It is well known that major SEP events are associated with intense episodes of solar activity when one or more active regions on the Sun produce a series of CMEs [e.g., *Jiggens and Gabriel*, 2009; *Ruzmaikin et al.*, 2011]. Therefore, the presence of a preceding CME in interplanetary (IP) space when the injection of SEPs by an unrelated solar event occurs is not an infrequent circumstance. The presence of a preceding CME in space has been suggested as a factor favoring the acceleration of particles by a shock driven by a second fast CME propagating in the wake of the preceding CME [*Gopalswamy et al.*, 2003; *Li et al.*, 2012; *Ding et al.*, 2013]. Both the turbulent enhancement generated downstream of the preceding CME and the presence of a suprathermal particle population accelerated by the shock driven by the preceding CME provide propitious conditions for an efficient acceleration of particles by the shock driven by the trailing CME associated with the origin of the SEP event (also known as the primary CME) [e.g., *Li et al.*, 2012]. The presence of a preceding CME in IP space, however, may also affect the transport of SEPs by

introducing changes in the direction and strength of the magnetic field surrounding it and increasing the level of magnetic turbulence in the IP medium [e.g., *Hundhausen*, 1972; *Vandas et al.*, 1996]. SEPs injected into such a distorted medium must propagate undergoing scattering and mirroring processes produced by the enhanced level of magnetic field compressions, discontinuities, and turbulence created in the wake of the preceding CME [e.g., *Hudson*, 1965; *Vandas et al.*, 1996]. These transport effects may have evident consequences in the measured SEP intensities depending on where the observer is located with respect to the preceding CME [e.g., *Lario et al.*, 2008].

The presence of a CME in the IP medium (hereafter ICME) at the time of the injection of SEPs has been suggested as a factor favoring the observation of the most intense SEP events [*Kallenrode and Cliver*, 2001]. A possible mechanism proposed by *Kallenrode* [2001, 2002] to explain these elevated particle intensities consists in the presence of a magnetic barrier in IP medium (created by a preceding ICME) able to affect the transport of SEPs accelerated by a second fast CME-driven shock by introducing processes of magnetic reflection and trapping. Energetic particles accelerated by the second fast CME-driven shock remain then confined between the magnetic barrier and the second fast CME-driven shock [*Kallenrode*, 2001, 2002]. When this magnetic barrier created by a preceding ICME is located beyond the observer's location, particles injected by the second fast CME-driven shock (i.e., the primary CME) may be reflected and/or scattered back to the observer, resulting in particle intensities higher than the intensities observed in the case when particle injection occurs in a pristine undisturbed solar wind medium [*Lario et al.*, 2008]. In order to efficiently affect the transport of SEPs, the preceding ICME must not only introduce changes in the direction and strength of the magnetic field where particles propagate, but increase the level of magnetic field turbulence to enhance the scattering processes undergone by the particles and thus rearrange the pitch angle distribution of the particles that eventually will be mirrored back toward the observer.

If the preceding ICME is located between the Sun and the observer, one may predict that the IP disturbances produced by the ICME may act as intervening structures for the newly fresh particles injected by the primary CME-driven shock, resulting then in both a delay in the arrival of particles at the observer and an attenuated particle intensity with respect to what the injection of SEPs into a pristine IP medium would have produced [e.g., *Lario et al.*, 2008]. Besides, if the preceding ICME has a magnetic structure consisting of looped field lines rooted to the Sun, the injection of SEPs onto one of these looped field lines (usually characterized by a low level of magnetic field turbulence) results in particles moving back and forth along these looped field lines [*Richardson and Cane*, 1996]. The confinement of particles into such looped structures will then result in elevated particle intensities but only if the observer intercepts such a structure when the SEP injection occurs or when intensities have not decreased significantly due to the expansion of the ICME [e.g., *Lario*, 2006, and references therein].

In this article, we study in a statistical sense whether the presence of prior ICMEs plays a role in the particle intensities measured early in the SEP events. We combine the list of SEP events observed near-Earth during solar cycle 23 compiled by *Cane et al.* [2010] with the list of near-Earth ICMEs compiled by Richardson and Cane [www.srl.caltech.edu/ACE/ASC/DATA/level3/icmetable2.htm] and the catalog of CMEs observed by the Large Angle and Spectrometric Coronagraph (LASCO) on board the Solar Heliospheric Observatory (SOHO) compiled by S. Yashiro [cdaw.gsfc.nasa.gov/CME_list] to determine whether the SEP events were observed under either disturbed or undisturbed solar wind conditions caused by the presence of prior ICMEs and in the case of disturbed conditions whether the transient structures (i.e., preceding ICMEs) were located either between the Sun and Earth or beyond Earth. Over the ensemble of events, we find that the most intense SEP events are observed when Earth is located within an ICME, followed by events observed in the downstream region of an ICME. By contrast, the injection of SEPs when an ICMEs is located between the Sun and the observer (i.e., when an ICME, unrelated to the origin of the SEP event, is observed after the onset of the SEP event) results in SEP events that tend to have lower averaged proton peak intensities. As described below, the arrival of an ICME near Earth shortly following the onset of a SEP event does not necessarily imply that the propagation of SEPs toward Earth was affected by the presence of this ICME. Therefore, we have studied also the possibility that a preceding CME observed by coronagraphs and ejected from the same source region that generated the SEP event has a significant effect in the acceleration and transport of SEPs and consequently in the observed SEP intensities. We find that the possible effect of this preceding CME impeding the transport of SEPs between the Sun and the observer has a smaller influence in the measured SEP peak intensities than the effects produced by preceding ICMEs located at or beyond the observer, and that

the effects that preceding CMEs from the same active region have in preconditioning the medium for an efficient acceleration of particles by a fast primary CME are still significant with respect to transport effects.

The structure of the article is as follows. In section 2 we describe the data sources and the classification of the SEP events in terms of the presence or absence of prior ICMEs and the presence or absence of preceding coronagraph CMEs. In section 3 we study the possible dependence between particle peak intensities and either the speed of the associated CMEs or the peak intensities of the associated soft X-ray flares. In section 4 we analyze the possible dependence between SEP peak intensities and the conditions of the IP medium (either quiet or perturbed) where the SEP event develops. Finally, in section 5 we present the main conclusions of the work.

## 2. Data and SEP Event Classification

We use the list of SEP events compiled by *Cane et al.* [2010] who selected proton events observed near Earth at energies above ~25 MeV in the years 1997–2006 with peak proton intensity in the ~20–30 MeV range above $2 \times 10^{-4}$ particles $(\text{cm}^2\ \text{sr}\ \text{s}\ \text{MeV})^{-1}$ and that were not compromised by data gaps and other events. A total of 280 events were selected by *Cane et al.* [2010] using data from the Goddard Space Flight Center (GSFC) experiment on the Interplanetary Monitoring Platform-J (IMP-8) and the University of Turku Energetic and Relativistic Nuclei and Electron (ERNE) experiment on board SOHO. In a few cases, they also used the GSFC Energetic Particle Acceleration Composition and Transport (EPACT) experiment on Wind. In this work we have considered the same set of events previously identified by *Cane et al.* [2010] but now using hourly averages of 175–315 keV electron intensities measured by the Electron Proton and Alpha Monitor (EPAM) on board the Advanced Composition Explorer (ACE) [*Gold et al.*, 1998] and 9–15, 15–40, 40–80 MeV proton intensities measured by the Energetic Particle Sensor (EPS) on board the Geostationary Operation Environmental Satellites (GOES) [*Sauer*, 1993; *Onsager et al.*, 1996].

In order to minimize the longitudinal dependence of SEP peak intensities [e.g., *Lario et al.*, 2006, 2013] and still having a significant number of events to study, we have chosen, among the SEP events selected by *Cane et al.* [2010], those generated from longitudes between W10° and W110°. This range of longitudes covers those events generated within ±50° from the footpoint of a nominal Parker spiral magnetic field line connecting Earth with the Sun (assuming a solar wind speed of ~400 km $\text{s}^{-1}$). Out of the 280 proton events identified by *Cane et al.* [2010], we have kept 147 SEP events associated with solar flares in the longitudinal range W10°–W110° for which we have been able to identify the peak intensity of the event in their prompt component, understood as the maximum intensity observed shortly after the onset of the event and several hours or days before the particle enhancement commonly associated with the arrival of interplanetary shocks (if any). The peak intensity in the prompt component is usually reached when the associated CME-driven shock is still close to the Sun and presumably able to accelerate protons and electrons to high energies. For some events, the maximum intensity in the prompt component is observed in the form of a plateau in the time-intensity profile before the local enhancement associated with the passage of shocks [*Reames and Ng*, 1998]. In these cases, the peak intensity is taken as the maximum value of the intensity plateau. Spacecraft observations for which particle intensity continuously increases until the arrival of the shock (if any) are excluded from our statistical study.

Table 1 provides the list of events selected for our statistical study. Column 1 gives an index that numbers the SEP event. Columns 2 and 3 provide the onset times of the proton intensities to the nearest hour as identified by *Cane et al.* [2010]. The date (and day of year in parenthesis) is that of the associated flare so that if the particle intensities rise on the following day the hour can be >23. Columns 4–6 provide the parameters of the associated flares; i.e., the onset of the soft X-ray emission, H$\alpha$ location and the GOES soft X-ray class ($F_{SXR}$) as identified by *Cane et al.* [2010]. When an event was behind the limb but had an associated soft X-ray event, *Cane et al.* [2010] estimated the longitude from the time since a probably associated active region went over the limb, otherwise a longitude of W120 was assigned. The events for which *Cane et al.* [2010] assigned a longitude >W110° are excluded from our analysis. Columns 7 and 8 provide the first observing time and the sky-plane speed (in km $\text{s}^{-1}$) of the associated parent CME as observed by LASCO as reported in Table 1 of *Cane et al.* [2010] and validated with the Coordinated Data Analysis Workshops (CDAW) CME catalog posted on cdaw.gsfc.nasa.gov/CME_list.

**Table 1.** SEP Events (Sep 1997–Dec 2006)

| Event | Onset Proton Event[a] | | Flare Event[b] | | | CME[c] | | Event | $t_{max}$ | Peak[f] | Peak[f] | Peak[f] | Peak[f] | Prec. |
|---|---|---|---|---|---|---|---|---|---|---|---|---|---|---|
| # | Day of Year | Hour | Onset | Site | $F_{SXR}$ | Time | $V_{CME}$ | Class[d] | DE4[e] | DE4 | P3 | P4 | P5 | CME[g] |
| (1) | (2) | (3) | (4) | (5) | (6) | (7) | (8) | (9) | (10) | (11) | (12) | (13) | (14) | (15) |
| | | | | | | | *1997* | | | | | | | |
| 1 | 3 Nov (307) | 11 | 1018 | 17°S, 22°W | M4.2 | 1111 | 352 | 0,0,-,- | 307/2100 | 5.95E1 | 3.52E−2 | – | – | P |
| 2 | 4 Nov (308) | 07 | 0552 | 14°S, 33°W | X2.1 | 0610 | 785 | 0,0,0,0 | 308/0900 | 4.12E3 | 3.85E0 | 1.51E0 | 2.24E−1 | P |
| 3 | 6 Nov (310) | 12 | 1149 | 18°S, 63°W | X9.4 | 1210 | 1556 | 1,2,2,1 | 310/1700 | 3.41E4 | 2.73E1 | 1.31E1 | 2.34E0 | NP[h] |
| 4 | 13 Nov (317) | 23 | ? | N, 110°W | ? | 2225 | 546 | 0,0,0,0 | 317/2300 | 8.25E2 | 1.64E−1 | 5.12E−2 | 4.37E−3 | – |
| | | | | | | | *1998* | | | | | | | |
| 5 | 26 Jan (026) | 23 | 2219 | 17°S, 55°W | C5.4 | 2327 | 399 | 1,1,1,- | 027/0000 | 2.57E2 | 4.88E−2 | 9.82E−3 | – | NP |
| 6 | 20 Apr (110) | 12 | 0938 | S, 90°W | M1.4 | 1007 | 1863 | 0,0,0,0 | 110/1300 | 5.81E3 | 1.65E1 | 1.27E1 | 1.09E−1 | NP[h,i] |
| 7 | 2 May (122) | 14 | 1331 | 15°S, 15°W | X1.1 | 1406 | 938 | 3,3,3,3 | 122/1600 | 9.35E3 | 6.63E0 | 3.95E0 | 4.84E−1 | P |
| 8 | 6 May (126) | 08 | 0758 | 11°S, 65°W | X2.7 | 0829 | 1099 | 3,3,3,3 | 126/0800 | 3.13E4 | 1.35E1 | 7.60E0 | 3.85E−1 | P |
| 9 | 9 May (129) | 05 | 0304 | S, 100°W | M7.7 | 0335 | 2331 | 4,4,4,4 | 129/1200 | 7.68E2 | 3.50E−1 | 1.63E−1 | 1.58E−2 | – |
| 10 | 27 May (147) | 15 | 1313 | 21°S, 83°W | C7.5 | 1345 | 878 | 0,-,-,- | 147/1600 | 5.84E2 | – | – | – | NP |
| 11 | 6 Sep (249) | 07 | 0454 | 21°S, 36°W | C1.3 | dg | dg | 0,0,0,0 | 249/0800 | 1.08E2 | 9.24E−2 | 2.39E−2 | 2.79E−3 | dg |
| 12 | 9 Sep (252) | 06 | 0452 | 21°S, 75°W | M2.8 | dg | dg | 0,0,0,- | 252/0600 | 1.20E2 | 6.40E−2 | 1.23E−2 | – | dg |
| 13 | 27 Sep (270) | 09 | 0806 | 21°N, 48°W | C2.6 | dg | dg | 4,4,4- | 270/0900 | 1.76E3 | 8.01E−2 | 6.97E−3 | – | dg |
| 14 | 30 Sep (273) | 14 | 1304 | 19°N, 85°W | M2.8 | dg | dg | 0,0,0,0 | 273/2200 | 1.95E4 | 1.00E2 | 2.99E1 | 1.28E0 | dg |
| 15 | 5 Nov (309) | <22 | 1900 | 26°N, 18°W | M8.4 | 2044 | 1118 | 1,1,1,- | 310/2000 | 1.93E2 | 1.80E0 | 6.78E−2 | – | P |
| 16 | 22 Nov (326) | 08 | 0630 | 27°S, 82°W | X3.7 | dg | dg | 0,0,0,0 | 326/0800 | 8.02E1 | 1.56E−1 | 8.51E−2 | 1.30E−2 | dg |
| 17 | 24 Nov (328) | 03 | 0207 | S, 108°W | X1.0 | 0230 | 1798 | 0,0,0,0 | 328/0900 | 2.62E2 | 1.05E−1 | 3.98E−2 | 6.94E−3 | dg |
| 18 | 17 Dec (351) | 11 | 0740 | 27°S, 46°W | M3.2 | 0830 | 302 | 0,-,-,- | 351/1000 | 7.19E1 | – | – | – | NP |
| | | | | | | | *1999* | | | | | | | |
| 19 | 3 Jan (003) | 16 | 1449 | 23°S, 49°W | C6.2 | dg | dg | 1,1,-,- | 003/2000 | 3.05E1 | 4.60E−2 | – | – | dg |
| 20 | 6 Jan (006) | 25 | 2354 | S, 95°W | C8.0 | dg | dg | 4,-,-,- | 007/0100 | 4.67E1 | – | – | – | dg |
| 21 | 16 Feb (047) | 06 | 0249 | 23°S, 14°W | M3.2 | dg | dg | 5,5,-,- | 047/0600 | 3.90E1 | 3.05E−2 | – | – | dg |
| 22 | 9 May (129) | 19 | 1753 | N, 95°W | M7.6 | 1827 | 615 | 0,0,0,0 | 129/1800 | 1.96E2 | 1.94E−1 | 4.50E−2 | 3.61E−2 | – |
| 23 | 4 Jun (155) | 08 | 0652 | 17°N, 69°W | M3.9 | 0726 | 2221 | 4,4,4,4 | 155/0900 | 5.13E3 | 6.36E0 | 1.11E0 | 3.05E−2 | NP |
| 24 | 27 Jun (178) | 11 | 0834 | 22°N, 26°W | M1.0 | 0906 | 903 | 2,2,2,- | 178/1300 | 1.49E2 | 2.42E−2 | 4.76E−3 | – | P |
| 25 | 28 Aug (240) | 20 | 1752 | 26°S, 14°W | X1.1 | 1826 | 462 | 0,-,-,- | 240/1900 | 2.75E1 | – | – | – | P |
| 26 | 28 Dec (362) | 02 | 0039 | 20°N, 56°W | M4.5 | 0054 | 672 | 4,4,4,- | 362/0500 | 1.12E3 | 2.73E−2 | 1.03E−2 | – | P |
| | | | | | | | *2000* | | | | | | | |
| 27 | 12 Feb (043) | 05 | 0351 | 26°N, 24°W | M1.7 | 0431 | 1107 | 2,2,2,2 | 043/0600 | 8.80E1 | 1.99E−1 | 3.86E−2 | 2.37E−3 | P |
| 28 | 2 Mar (062) | 09 | 0820 | 14°S, 52°W | X1.1 | 0854 | 776 | 4,4,4,4 | 062/1000 | 2.44E2 | 2.87E−2 | 1.51E−2 | 2.29E−3 | NP |
| 29 | 3 Mar (063) | 03 | 0208 | 15°S, 60°W | M3.8 | 0230 | 841 | 4,4,4,4 | 063/0300 | 2.32E2 | 3.15E−2 | 8.33E−3 | 2.23E−3 | P |
| 30 | 22 Mar (082) | 20 | 1834 | 14°N, 57°W | X1.1 | 1931 | 478 | 0,0,0,- | 082/2200 | 7.23E1 | 1.70E−1 | 1.58E−2 | – | NP |
| 31 | 24 Mar (084) | 10 | 0741 | 15°N, 82°W | X1.8 | dg | dg | 0,-,-,- | 084/2300 | 4.51E1 | – | – | – | dg |
| 32 | 4 Apr (095) | 16 | 1512 | 16°N, 66°W | C9.7 | 1632 | 1188 | 0,0,0,0 | 095/1600 | 6.23E2 | 1.17E1 | 5.55E−1 | 5.96E−3 | NP |
| 33 | 27 Apr (118) | 16 | 1404 | N, 95°W | B9.8 | 1430 | 1110 | 0,0,0,- | 118/1900 | 1.87E1 | 4.28E−2 | 5.50E−3 | – | – |
| 34 | 1 May (122) | 11 | 1016 | 20°N, 54°W | M1.1 | 1054 | 1360 | 1,-,1,- | 122/1000 | 6.61E2 | – | 1.31E−2 | – | NP |
| 35 | 4 May (125) | 12 | 1057 | 20°S, 90°W | M6.8 | 1126 | 1404 | 3,-,-,- | 125/1600 | 4.58E2 | – | – | – | P |
| 36 | 15 May (136) | 18 | 1546 | 22°S, 68°W | C7.8 | 1626 | 1212 | 5,3,3,- | 136/1800 | 5.94e2 | 1.90E−1 | 2.52E−2 | – | NP |
| 37 | 23 May (144) | 22 | 2048 | 23°N, 41°W | C9.5 | 2130 | 475 | 5,5,-,- | 144/2300 | 2.94E2 | 3.08E−2 | – | – | NP |
| 38 | 10 Jun (162) | 18 | 1640 | 22°N, 40°W | M5.2 | 1708 | 1108 | 5,5,5,5 | 162/1700 | 3.31E3 | 3.51E0 | 1.15E0 | 1.44E−1 | NP |
| 39 | 15 Jun (167) | 21 | 1938 | 20°N, 62°W | M1.8 | 1950 | 1081 | 4,-,-,- | 167/2100 | 2.88E2 | – | – | – | NP |
| 40 | 17 Jun (169) | 05 | 0225 | 22°N, 72°W | M3.5 | 0328 | 927 | 5,5,5,- | 169/0500 | 8.13E2 | 8.17E−2 | 1.85E−2 | – | NP |
| 41 | 18 Jun (170) | 26 | 0152 | 23°N, 85°W | X1.0 | 0210 | 629 | 1,1,1,1 | 170/0300 | 6.44E2 | 4.12E−1 | 6.24E−2 | 3.35E−3 | P |
| 42 | 23 Jun (175) | 16 | 1418 | 23°N, 72°W | M3.0 | 1454 | 847 | 2,2,2,2 | 175/1500 | 1.55E3 | 1.55E−1 | 2.93E−2 | 2.22E−3 | P |
| 43 | 25 Jun (177) | 12 | 0717 | 16°N, 55°W | M1.9 | 0754 | 1617 | 3,3,3,- | 177/1300 | 5.47E1 | 1.58E−1 | 2.33E−2 | – | NP |
| 44 | 28 Jun (180) | 20 | 1848 | N, 95°W? | C3.7 | 1931 | 1198 | 4,4,-,- | 180/2000 | 4.31E1 | 3.10E−2 | – | – | – |
| 45 | 22 Jul (204) | 12 | 1117 | 14°N, 56°W | M3.7 | 1154 | 1230 | 5,5,5,5 | 204/1200 | 1.19E3 | 1.29E0 | 4.49E−1 | 4.82E−2 | NP |
| 46 | 12 Aug (225) | 11 | 0945 | 17°S, 79°W | M1.1 | 1035 | 662 | 3,3,3,- | 225/1600 | 2.84E2 | 1.80E−1 | 1.78E−2 | – | NP |
| 47 | 7 Sep (251) | 21 | 2032 | 06°N, 47°W | C7.2 | 2130 | 422 | -,1,1,- | 252/0400[k] | – | 3.97E−2 | 6.12E−3 | – | NP |
| 48 | 9 Sep (253) | 10 | 0828 | 07°N, 67°W | M1.6 | 0856 | 554 | 3,3,3,- | 253/1100 | 7.07E1 | 4.86E−2 | 1.31E−2 | – | P |
| 49 | 19 Sep (263) | 11 | 0806 | 14°N, 46°W | M5.1 | 0850 | 766 | 3,3,3,- | 263/1300 | 2.62E4 | 9.35E−2 | 1.51E−2 | – | P |
| 50 | 9 Oct (283) | <30 | 2319 | 01°N, 14°W | C6.7 | 2350 | 798 | 0,0,0,- | 285/1200 | 2.20E1 | 4.85E−2 | 1.01E−2 | – | P |
| 51 | 16 Oct (290) | 07 | 0640 | N, 95°W | M2.5 | 0727 | 1336 | 4,4,4,4 | 290/0900 | 4.83E2 | 1.30E0 | 3.98E−1 | 4.67E−2 | – |
| 52 | 8 Nov (313) | 23 | 2242 | 10°N, 75°W | M7.4 | 2306 | 1738 | 3,3,3,3 | 314/0100 | 3.00E5 | 4.43E2 | 3.97E2 | 6.65E1 | NP[h,i] |

**Table 1.** (continued).

| Event | Onset Proton Event[a] | | Flare Event[b] | | | CME[c] | | Event | $t_{max}$ | Peak[f] | Peak[f] | Peak[f] | Peak[f] | Prec. |
|---|---|---|---|---|---|---|---|---|---|---|---|---|---|---|
| # | Day of Year | Hour | Onset | Site | $F_{SXR}$ | Time | $V_{CME}$ | Class[d] | DE4[e] | DE4 | P3 | P4 | P5 | CME[g] |
| (1) | (2) | (3) | (4) | (5) | (6) | (7) | (8) | (9) | (10) | (11) | (12) | (13) | (14) | (15) |
| | | | | | | | *2001* | | | | | | | |
| 53 | 26 Jan (026) | 14 | 1150 | 27°S, 57°W | C1.6 | 1206 | 928 | 4,4,4,- | 026/1400 | 4.80E1 | 7.38E−2 | 8.23E−3 | – | NP |
| 54 | 28 Jan (028) | 17 | 1540 | 04°S, 59°W | M1.5 | 1554 | 916 | 4,4,4,4 | 028/1900 | 1.60E3 | 6.03E0 | 5.70E−1 | 6.66E−2 | P |
| 55 | 11 Feb (042) | 03 | 0057 | 24°N, 57°W | C6.5 | 0131 | 1183 | 0,0,0,- | 042/1100 | 1.01E2 | 7.47E−2 | 1.37E−2 | – | NP |
| 56 | 10 Mar (069) | 08 | 0400 | 27°N, 42°W | M6.7 | 0426 | 819 | 0,-,-,- | 069/0900 | 2.77E2 | – | – | – | NP |
| 57 | 29 Mar (088) | 12 | 0957 | 16°N, 12°W | X1.7 | 1026 | 942 | 3,3,3,3 | 088/1600 | 3.31E3 | 3.74E0 | 8.62E−1 | 4.05E−2 | P |
| 58 | 2 Apr (092) | 13 | 1058 | 16°N, 62°W | X1.1 | 1126 | 992 | 3,3,3,3 | 092/1700 | 9.80E2 | 2.81E−1 | 9.06E−2 | 8.10E−3 | NP |
| 59 | 2 Apr (092) | 23 | 2132 | 17°N, 72°W | X20 | 2206 | 2505 | 3,3,3,3 | 093/0400 | 2.41E4 | 4.64E1 | 2.09E1 | 1.91E0 | P |
| 60 | 12 Apr (102) | 12 | 0939 | 20°S, 42°W | X2.0 | 1031 | 1184 | 3,3,3,3 | 102/1300 | 6.03E3 | 3.07E0 | 1.27E0 | 1.48E−1 | P |
| 61 | 14 Apr (104) | 18 | 1715 | 17°S, 71°W | M1.0 | 1754 | 830 | 5,5,-,- | 104/1800 | 3.11E3 | 2.08E−1 | – | – | P |
| 62 | 15 Apr (105) | 14 | 1319 | 20°S, 84°W | X14 | 1406 | 1199 | 5,3,3,3 | 105/1600 | 5.43E4 | 5.42E1 | 2.76E1 | 3.52E0 | P |
| 63 | 26 Apr (116) | <22 | 1126 | 17°N, 31°W | M7.8 | 1230 | 1006 | 0,8,8,- | 116/1500 | 5.86E1 | −8.88E8 | −8.88E8 | – | P |
| 64 | 20 May (140) | 08 | 0600 | 17°S, 91°W | M6.5 | 0626 | 546 | 0,0,0,0 | 140/0900 | 5.64E2 | 3.53E−1 | 1.94E−1 | 3.07E−2 | – |
| 65 | 4 Jun (155) | 17 | 1611 | 22°N, 60°W | C3.2 | 1630 | 464 | 0,0,0,0 | 155/1700 | 8.40E1 | 2.33E−1 | 4.74E−2 | 3.24E−3 | NP |
| 66 | 11 Jun (162) | <14 | 0533 | 16°S, 34°W? | C7.1 | 0606 | 326 | 0,0,-,- | 162/2300 | 5.59E1 | 3.57E−2 | – | – | NP |
| 67 | 18 Jun (169) | 27 | 2150 | 10°S, 23°W | C4.7 | 2246 | 1301 | 0,0,0,0 | 170/0600 | 1.50E2 | 4.79E−2 | 1.02E−2 | 4.20E−3 | NP |
| 68 | 19 Jul (200) | 11 | 0952 | 12°S, 62°W | M1.8 | 1030 | 1668 | 0,-,-,- | 200/1400 | 1.83E2 | – | – | – | NP |
| 69 | 14 Aug (226) | 18 | 1130 | 110°W | C2.3 | 1601 | 618 | 1,1,1,- | 227/0000 | 5.51E1 | 8.45E−2 | 1.25E−2 | – | – |
| 70 | 12 Sep (255) | 23 | ? | 16°S, 62°W? | C9.6 | 2206 | 668 | 1,1,-,- | 255/1600 | 9.66E1 | 3.39E−2 | – | – | NP |
| 71 | 15 Sep (258) | 12 | 1104 | 27°S, 53°W | M1.5 | 1154 | 478 | 4,4,4,4 | 258/1300 | 2.07E2 | 1.11E0 | 2.23E−1 | 8.31E−3 | NP |
| 72 | 1 Oct (274) | <12 | 0441 | S, 95°W | M9.1 | 0530 | 1405 | 8,3,3,3 | 274/2200[k] | −8.88E8 | 4.50E1 | 1.72E1 | 7.76E−1 | – |
| 73 | 5 Oct (278) | <17 | ? | S, 110°W | C2.0 | 1030 | 1537 | 4,4,4,4 | 279/0900 | 7.35E2 | 8.31E−1 | 1.63E−1 | 3.96E−3 | – |
| 74 | 19 Oct (292) | 01 | 0047 | 16°N, 18°W | X1.8 | 0127 | 558 | 0,0,0,0 | 292/0500 | 2.59E2 | 5.42E−1 | 1.45E−1 | 1.43E−2 | P |
| 75 | 19 Oct (292) | 16 | 1613 | 15°N, 29°W | X1.6 | 1650 | 901 | 0,0,0,0 | 292/1800 | 4.53E2 | 9.89E−1 | 2.56E−1 | 2.69E−2 | P |
| 76 | 22 Oct (295) | 04 | 0022 | 17°N, 57°W | M1.0 | 0050 | 772 | 3,-,-,- | 295/0500 | 8.96E1 | – | – | – | NP |
| 77 | 4 Nov (308) | 17 | 1603 | 06°N, 18°W | X1.0 | 1635 | 1810 | 5,5,5,5 | 309/0300 | 9.35E4 | 1.26E2 | 1.01E2 | 1.44E1 | NP[j] |
| 78 | 26 Dec (360) | 06 | 0432 | 08°N, 54°W | M7.1 | 0530 | 1446 | 0,0,0,0 | 360/0700 | 2.31e4 | 4.77E1 | 2.16E1 | 4.42E0 | NP[h] |
| | | | | | | | *2002* | | | | | | | |
| 79 | 14 Jan (014) | <08 | 0529 | S, 100°W | M4.4 | 0540 | 1492 | 0,0,0,0 | 015/2000 | 1.67E3 | 2.01E0 | 3.32E−1 | 1.35E−2 | – |
| 80 | 20 Feb (051) | 06 | 0552 | 12°N, 72°W | M5.1 | 0630 | 952 | 0,0,0,0 | 051/0600 | 3.33E3 | 8.82E−1 | 2.96E−1 | 1.18E−2 | NP |
| 81 | 22 Mar (081) | 12 | 1012 | S, 90°W | M1.6 | 1106 | 1750 | 5,5,5,- | 081/1400 | 9.50E1 | 3.23E0 | 8.61E−2 | – | NP |
| 82 | 11 Apr (101) | 16 | 1616 | 15°S, 33°W | C9.2 | 1650 | 540 | 1,1,1,- | 101/1800 | 1.26E2 | 1.30E−1 | 2.09E−2 | – | NP |
| 83 | 14 Apr (104) | 12 | 0728 | 19°N, 57°W | C9.6 | 0750 | 757 | 4,-,-,- | 104/1400 | 3.91E1 | – | – | – | NP |
| 84 | 15 Apr (105) | 03 | 0246 | 19°N, 79°W | C9.8 | 0306 | 674 | 4,-,-,- | 105/0300 | 1.82E2 | – | – | – | P |
| 85 | 17 Apr (107) | 08 | 0746 | 14°S, 34°W | M2.6 | 0826 | 1240 | 2,3,3,3 | 107/1200 | 5.57E3 | 1.59E0 | 2.98E−1 | 7.96E−3 | NP |
| 86 | 21 Apr (111) | 00 | 0043 | 14°S, 84°W | X1.5 | 0127 | 2393 | 3,4,3,3 | 111/1300 | 3.50E4 | 2.33E2 | 7.66E1 | 9.21E0 | NP[i] |
| 87 | 22 May (142) | 06 | 0318 | 22°S, 53°W | C5.0 | 0350 | 1557 | 4,4,4,4 | 142/0900 | 1.36E2 | 5.20E−1 | 1.06E−1 | 3.04E−3 | P |
| 88 | 30 May (150) | 03 | 0424 | N, 100°W | M1.3 | 0506 | 1625 | 0,-,-,- | 150/0800 | 1.02E2 | – | – | – | – |
| 89 | 7 Jul (188) | 12 | 1115 | S, 95°W | M1.0 | 1130 | 1423 | 0,0,0,0 | 188/1600 | 3.27E3 | 1.79E0 | 5.98E−1 | 2.31E−2 | – |
| 90 | 3 Aug (215) | 19 | 1859 | 16°S, 76°W | X1.0 | 1932 | 1150 | 3,4,4,- | 216/0100 | 3.02E2 | 3.79E−2 | 8.24E−3 | – | NP |
| 91 | 5 Aug (217) | 07 | ? | 07°S, 45°W? | C2.0 | 0732 | 689 | 4,-,-,- | 217/0800 | 4.13E2 | – | – | – | P |
| 92 | 14 Aug (226) | 03 | 0147 | 09°N, 54°W | M2.3 | 0230 | 1309 | 0,0,0,0 | 226/0200 | 2.37E3 | 5.57E0 | 1.93E−1 | 3.80E−3 | NP |
| 93 | 16 Aug (228) | 07 | 0546 | 06°N, 83°W | M2.9 | 0606 | 1378 | 0,0,0,0 | 228/0800 | 5.63E2 | 4.57E−2 | 1.43E−2 | 3.05E−3 | P |
| 94 | 18 Aug (230) | 20 | 2112 | 12°S, 19°W | M2.2 | 2154 | 682 | 2,2,2,2 | 230/2200 | 1.10E3 | 5.10E−1 | 7.11E−2 | 4.75E−3 | NP |
| 95 | 19 Aug (231) | 10 | 1028 | 12°S, 25°W | M2.0 | 1106 | 549 | 2,-,-,- | 231/1100 | 4.36E3 | – | – | – | P |
| 96 | 20 Aug (232) | 08 | 0822 | 10°S, 38°W | M3.4 | 0854 | 1099 | 3,3,3,3 | 232/0900 | 1.19E4 | 1.95E−1 | 5.03E−2 | 5.03E−3 | P |
| 97 | 22 Aug (234) | 02 | 0147 | 07°S, 62°W | M5.4 | 0206 | 998 | 4,4,4,4 | 234/0400 | 1.77E3 | 2.42E0 | 8.72E−1 | 1.23E−1 | P |
| 98 | 24 Aug (236) | 00 | 0049 | 02°S, 81°W | X3.1 | 0127 | 1913 | 4,4,4,4 | 236/0200 | 1.02E4 | 3.04E1 | 9.12E0 | 1.64E0 | P |
| 99 | 27 Sep (270) | 02 | 0118 | S, 95°W | C5.0 | 0154 | 1502 | 0,0,0,- | 270/0200 | 5.17E2 | 2.82E−2 | 6.11E−3 | – | – |
| 100 | 20 Oct (293) | 14 | 1410 | 13°S, 63°W | C6.6 | 1430 | 1011 | 0,-,-,- | 293/1400 | 2.75E2 | – | – | – | NP |
| 101 | 9 Nov (313) | 15 | 1308 | 12°S, 29°W | M4.6 | 1331 | 1838 | 0,0,0,0 | 314/0400 | 1.28E4 | 4.62E1 | 7.01E0 | 8.16E−2 | P |

**Table 1.** (continued).

| Event | Onset Proton Event[a] | | Flare Event[b] | | | CME[c] | | Event | $t_{max}$ | Peak[f] | Peak[f] | Peak[f] | Peak[f] | Prec. |
|---|---|---|---|---|---|---|---|---|---|---|---|---|---|---|
| # | Day of Year | Hour | Onset | Site | $F_{SXR}$ | Time | $V_{CME}$ | Class[d] | DE4[e] | DE4 | P3 | P4 | P5 | CME[g] |
| (1) | (2) | (3) | (4) | (5) | (6) | (7) | (8) | (9) | (10) | (11) | (12) | (13) | (14) | (15) |
| | | | | | | | *2003* | | | | | | | |
| 102 | 17 Mar (076) | 19 | 1850 | 14°S, 39°W | X1.5 | 1954 | 1020 | 0,0,-,- | 076/2000 | 4.17E2 | 7.90E−2 | – | – | Y |
| 103 | 18 Mar (077) | 14 | 1157 | 09°S, 46°W | X1.5 | 1354 | 1601 | 1,1,1,- | 077/1300 | 2.65E3 | 5.36E−2 | 1.33E−2 | – | P |
| 104 | 7 Apr (097) | <08 | 0925 | 10°S, 88°W | B7.3 | 0950 | 719 | 0,0,0,- | 097/1400 | 5.17E2 | 1.23E−1 | 8.82E−3 | – | P |
| 105 | 23 Apr (113) | 00 | 0045 | 22°N, 25°W | M5.1 | 0127 | 916 | 0,0,0,- | 113/0200 | 9.80E | 4.20E−2 | 1.67E−2 | – | P |
| 106 | 24 Apr (114) | 12 | 1245 | 21°N, 39°W | M3.3 | 1327 | 609 | 0,0,0,- | 114/1300 | 6.60E1 | 7.99E−2 | 2.57E−2 | – | P |
| 107 | 28 May (148) | 00 | 0017 | 06°S, 20°W | X3.6 | 0050 | 1366 | 0,8,8,0 | 148/1000[k] | 1.57E3 | −8.88E8 | −8.88E8 | 1.19E−2 | P |
| 108 | 31 May (151) | 03 | 0213 | 07°S, 65°W | M9.3 | 0230 | 1835 | 3,3,3,3 | 151/0500 | 9.37E3 | 2.00E0 | 6.44E−1 | 7.38E−2 | dg |
| 109 | 10 Jul (191) | 14 | 1354 | 13°N, 91°W | M3.6 | <1633 | 877 | 0,-,-,- | 191/1800 | 3.83E1 | – | – | – | dg |
| 110 | 19 Aug (231) | 03 | 0738 | 12°S, 64°W | M2.0 | 0830 | 412 | 3,3,-,- | 231/0900 | 3.23E2 | 4.14E−2 | – | – | Y |
| 111 | 26 Oct (299) | 18 | 1703 | 02°N, 38°W | X1.2 | 1754 | 1537 | 5,3,3,5 | 299/1900 | 1.04E4 | 4.28E1 | 1.03E1 | 4.00E−1 | P |
| 112 | 2 Nov (306) | 18 | 1703 | 14°S, 56°W | X8.0 | 1730 | 2598 | 4,4,4,4 | 306/1800 | 3.57E4 | 8.13E1 | 4.55E1 | 5.20E0 | P |
| 113 | 4 Nov (308) | 21 | 1929 | 19°S, 83°W | X28 | 1954 | 2657 | 4,0,0,0 | 308/2300 | 6.35E3 | 2.60E1 | 8.77E0 | 6.35E−1 | P |
| 114 | 7 Nov (311) | 16 | 1500 | S, 110°W | B4.7 | 1554 | 2237 | 0,0,0,- | 311/1800 | 1.26E3 | 7.84E−1 | 2.07E−1 | – | – |
| 115 | 20 Nov (324) | 07 | 0735 | 03°N, 12°W | M9.6 | 0806 | 669 | 2,3,3,3 | 324/1000 | 2.46E3 | 5.84E−1 | 1.04E−1 | 6.10E−3 | P |
| 116 | 2 Dec (336) | 12 | 1000 | S, 95°W | C7.2 | 1050 | 1393 | 0,0,0,- | 336/1200 | 1.51E2 | 1.50E1 | 1.88E0 | – | – |
| 117 | 31 Dec (365) | 18 | ? | ?99°W | M1.0 | dg | dg | 0,-,-,- | 365/1900 | 6.86E2 | – | – | – | – |
| | | | | | | | *2004* | | | | | | | |
| 118 | 4 Feb (035) | 11 | 1112 | 07°S, 49°W | C9.9 | 1154 | 764 | 0,-,-,- | 035/1300 | 9.05E1 | – | – | – | NP |
| 119 | 11 Apr (102) | 05 | 0354 | 16°S, 46°W | C9.6 | 0430 | 1645 | 0,0,0,0 | 102/0900 | 1.33E3 | 5.24E0 | 4.53E−1 | 1.32E−2 | NP |
| 120 | 13 Jul (195) | 01 | 0009 | 14°N, 59°W | M6.7 | 0054 | 409 | 0,0,0,- | 195/0200 | 6.37E1 | 9.68E−2 | 2.23E−2 | – | NP |
| 121 | 25 Jul (207) | 16 | 1419 | 04°N, 33°W | M1.1 | 1454 | 1333 | 5,3,3,3 | 207/1900 | 3.44E3 | 3.50E0 | 8.06E−1 | 1.49E−2 | P |
| 122 | 31 Jul (213) | <27 | 0516 | S, 95°W | C8.4 | 0554 | 1192 | 1,-,-,- | 213/1000 | 1.40E2 | – | – | – | – |
| 123 | 19 Sep (263) | 18 | 1646 | 03°N, 58°W | M1.9 | dg | dg | 3,3,3,3 | 263/1900 | 6.62E3 | 4.46E0 | 1.32E0 | 1.03E−1 | dg |
| 124 | 30 Oct (304) | 07 | 0608 | 13°N, 22°W | M4.2 | 0654 | 422 | 0,8,0,0 | 304/0800 | 9.16E2 | −8.88E8 | 2.17E−2 | 3.77E−3 | P |
| 125 | 30 Oct (304) | 13 | 1138 | 12°N, 26°W | X1.2 | 1230 | 427 | 0,0,8,- | 304/1300 | 3.38E3 | 1.50E−1 | -8.88E8 | – | P |
| 126 | 30 Oct (304) | 17 | 1618 | 13°N, 28°W | M5.9 | 1654 | 690 | 0,0,0,- | 304/1800 | 4.18E3 | 2.01E−1 | 4.85E−2 | – | P |
| 127 | 7 Nov (312) | 17 | 1542 | 09°N, 17°W | X2.0 | 1654 | 1759 | 2,3,3,3 | 312/2100 | 4.42E3 | 5.36E1 | 8.91E0 | 1.96E−1 | P |
| 128 | 9 Nov (314) | 19 | 1659 | 07°N, 51°W | M8.9 | 1726 | 2000 | 3,3,3,3 | 314/2000 | 4.21E3 | 9.23E0 | 1.49E0 | 3.61E−2 | NP |
| 129 | 10 Nov (315) | 03 | 0159 | 09°N, 49°W | X2.5 | 0226 | 2000 | 3,3,3,3 | 315/0900 | 5.90E3 | 2.22E1 | 7.70E0 | 4.56E−1 | P |
| | | | | | | | *2005* | | | | | | | |
| 130 | 17 Jan (017) | 10 | 0659 | 15°N, 25°W | X3.8 | 0954 | 2547 | 4,4,4,4 | 017/1700 | 1.81E5 | 1.96E2 | 1.16E2 | 1.73E1 | P |
| 131 | 20 Jan (020) | 06 | 0636 | 14°N, 61°W | X7.1 | 0654 | ~2500 | 4,4,4,4 | 020/0900 | 1.39E5 | 5.26E1 | 3.55E1 | 1.56E1 | P |
| 132 | 6 May (126) | 03 | 0305 | 04°S, 71°W | C9.3 | 0330 | 1120 | 0,0,0,- | 126/0400 | 9.17E2 | 2.10E−1 | 2.33E−2 | – | P |
| 133 | 6 May (126) | 12 | 1111 | 04°S, 76°W | M1.3 | 1154 | 1144 | 0,0,0,- | 126/1200 | 8.65E2 | 3.20E−1 | 2.60E−2 | – | P |
| 134 | 11 May (131) | 20 | 1922 | 10°S, 55°W | M1.1 | 2013 | 550 | 0,0,0,- | 131/2100 | 7.50E1 | 5.49E−2 | 1.11E−2 | – | P |
| 135 | 31 May (151) | 16 | 1433 | 12°N, 22°W | C2.4 | 1532 | 313 | 3,-,-,- | 151/1800 | 2.85E1 | – | – | – | NP |
| 136 | 14 Jun (165) | 06 | 0654 | 10°N, 48°W | C4.2 | 0724 | 791 | 2,-,-,- | 165/1900 | 5.03E1 | – | – | – | NP |
| 137 | 16 Jun (167) | 20 | 2001 | 09°N, 85°W | M4.0 | dg | dg | 3,3,3,3 | 167/2300 | 5.73E3 | 2.04E0 | 1.16E0 | 2.35E−1 | dg |
| 138 | 9 Jul (190) | 24 | 2147 | 11°N, 27°W | M2.8 | 2230 | 1540 | 2,2,2,2 | 191/0300 | 5.51E2 | 1.07E−1 | 3.54E−2 | 3.60E−3 | NP |
| 139 | 12 Jul (193) | 19 | 1547 | 11°N, 67°W | M1.5 | 1654 | 523 | 4,4,-,- | 193/1800 | 1.35E2 | 3.05E−2 | – | – | P |
| 140 | 13 Jul (194) | 05 | 0235 | 18°N, 82°W | M1.1 | 0306 | 759 | 4,-,-,- | 194/0700 | 1.20E2 | – | – | – | P |
| 141 | 13 Jul (194) | 14 | 1401 | 11°N, 78°W | M5.0 | 1430 | 1423 | 4,4,4,4 | 194/1600 | 2.26E3 | 1.43E0 | 2.48E−1 | 7.72E−3 | P |
| 142 | 14 Jul (195) | 11 | 1016 | 08°N, 89°W | X1.2 | 1030 | 2115 | 4,4,4,4 | 195/2200 | 5.80E3 | 1.24E1 | 3.93E0 | 1.43E−1 | P |
| 143 | 22 Aug (234) | 01 | 0044 | 09°S, 48°W | M2.6 | 0131 | 1194 | 0,0,0,0 | 234/0300 | 1.33E3 | 7.19E−1 | 1.41E−1 | 6.14E−3 | P |
| 144 | 22 Aug (234) | 18 | 1646 | 12°S, 60°W | M5.6 | 1730 | 2378 | 1,1,1,1 | 234/2300 | 1.29E4 | 3.80E1 | 8.36E0 | 2.52E−1 | P |

**Table 1.** (continued).

| Event | Onset Proton Event[a] | | Flare Event[b] | | | CME[c] | | Event | $t_{max}$ | Peak[f] | Peak[f] | Peak[f] | Peak[f] | Prec. |
|---|---|---|---|---|---|---|---|---|---|---|---|---|---|---|
| # | Day of Year | Hour | Onset | Site | $F_{SXR}$ | Time | $V_{CME}$ | Class[d] | DE4[e] | DE4 | P3 | P4 | P5 | CME[g] |
| (1) | (2) | (3) | (4) | (5) | (6) | (7) | (8) | (9) | (10) | (11) | (12) | (13) | (14) | (15) |
| | | | | | | | *2006* | | | | | | | |
| 145 | 6 Jul (187) | 09 | 0813 | 11°S, 32°W | M2.5 | 0854 | 911 | 0,0,0,0 | 187/1300 | 5.97E1 | 1.33E−1 | 4.98E−2 | 7.72E−3 | P |
| 146 | 13 Dec (347) | 02 | 0214 | 06°S, 23°W | X3.4 | 0254 | 1774 | 0,0,0,0 | 347/0500 | 4.78E4 | 2.43E1 | 2.01E1 | 5.83E0 | NP[h] |
| 147 | 14 Dec (348) | 22 | 2107 | 07°S, 46°W | X1.5 | 2230 | 1042 | 3,3,3,3 | 348/2300 | 2.35E3 | 1.35E1 | 4.68E0 | 3.71E−1 | NP[h] |

[a]Onset time of proton event as identified by *Cane et al.* [2010]. If the time is > 23 h then the time is the following day. Times preceded by < indicate that the event had a slow rise.

[b]Flare associated with the solar origin of the SEP event as identified by *Cane et al.* [2010], including the onset of the soft X-ray emission, the H$\alpha$ site, and the X-ray GOES class. A question mark indicates that no soft X-ray flare was observed.

[c]Primary CME associated with the origin of the SEP event, including the time of the first observation in LASCO coronagraphs and the plane-of-sky CME speed.

[d]Event class according to the criteria described in section 2.1 for the energy channels DE4 (175–315 keV electrons), P3 (9–15 MeV protons), P4 (15–40 MeV protons), and P5 (40–80 MeV protons). The symbol "–" indicates that no intensity enhancement is observed in that energy channel, and "8" that no peak intensity in the prompt component of the event has been identified.

[e]Time when the peak intensity in the prompt component of the event in the DE4 175–315 keV electron channel of ACE/EPAM was observed, in units of day of year/nearest hour.

[f]Peak intensity in the indicated energy channel (DE4 for 175–315 keV electrons, P3 for 9–15 MeV protons, P4 for 15–40 MeV protons, and P5 for 40–80 MeV protons) in units of particles $cm^{-2}$ $s^{-1}$ $sr^{-1}$ $MeV^{-1}$. The value −8.88E8 indicates that no peak intensity in the prompt component of the SEP event was identifiable.

[g]Event classification based on the criteria described in section 2.2. P indicates events with a preceding CME, NP without a CME listed in the CDAW catalog, and dg event occurring during a LASCO data gap.

[h]*Ding et al.* [2013] identified a preceding CME with a width < 60° within 9 h of the primary CME.

[i]*Gopalswamy et al.* [2004] determined that a major preceding eruption occurred from the same active region as the primary CME, but the primary CME followed so closely that would have overtaken the preceding CME within the occulting disk of LASCO.

[j]*Ding et al.* [2013] identified a wide (> 60°) preceding CME using the CACTuS database of CMEs but not listed in CDAW.

[k]The indicated time of maximum does not refer to the energy channel DE4 but to the lowest proton energy with an identifiable peak intensity.

### 2.1. SEP Event Classification Based on In Situ Observations of ICMEs

We propose a first classification scheme for the SEP events based on the presence or absence of ICMEs as determined from in situ observations of ICMEs. In order to determine the absence or presence of an ICME, we rely on the list of near-Earth ICMEs compiled by Richardson and Cane and posted on www.srl.caltech.edu/ACE/ASC/DATA/level3/icmetable2.htm. The criteria and parameters used by Richardson and Cane to identify the passage of near-Earth ICMEs are described in *Cane and Richardson* [2003] and *Richardson and Cane* [2010].

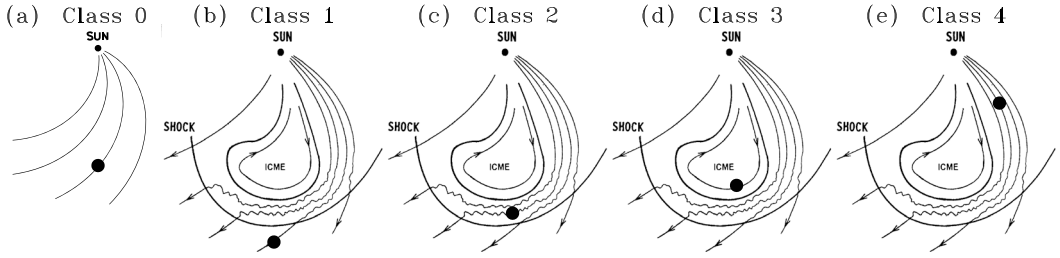


**Figure 1.** Schematic representation of the interplanetary environment where SEP events occur for Classes 0 to 4. The big solid black dot identifies the location of the observer when the peak intensity of the prompt component of the SEP event is observed. (a) Class 0 events occur under undisturbed solar wind conditions represented here by a nominal Parker spiral interplanetary magnetic field. If the peak intensity of the prompt component of the event is observed when (b) a prior ICME is located between the Sun and the observer, the SEP event is classified as Class 1; (c) when the observer is in the sheath region of a prior ICME, the SEP event is Class 2, (d) when the observer is within a prior ICME, the SEP event is Class 3, and (e) when the ICME is located beyond the spacecraft, the SEP event is Class 4. Class 5 events (not plotted) occur when two or more ICMEs are present in the interplanetary medium with one ICME located beyond the observer and another ICME between the Sun and the observer. The schematic Figures 1b–1e have been adapted from *Cane and Lario* [2006].

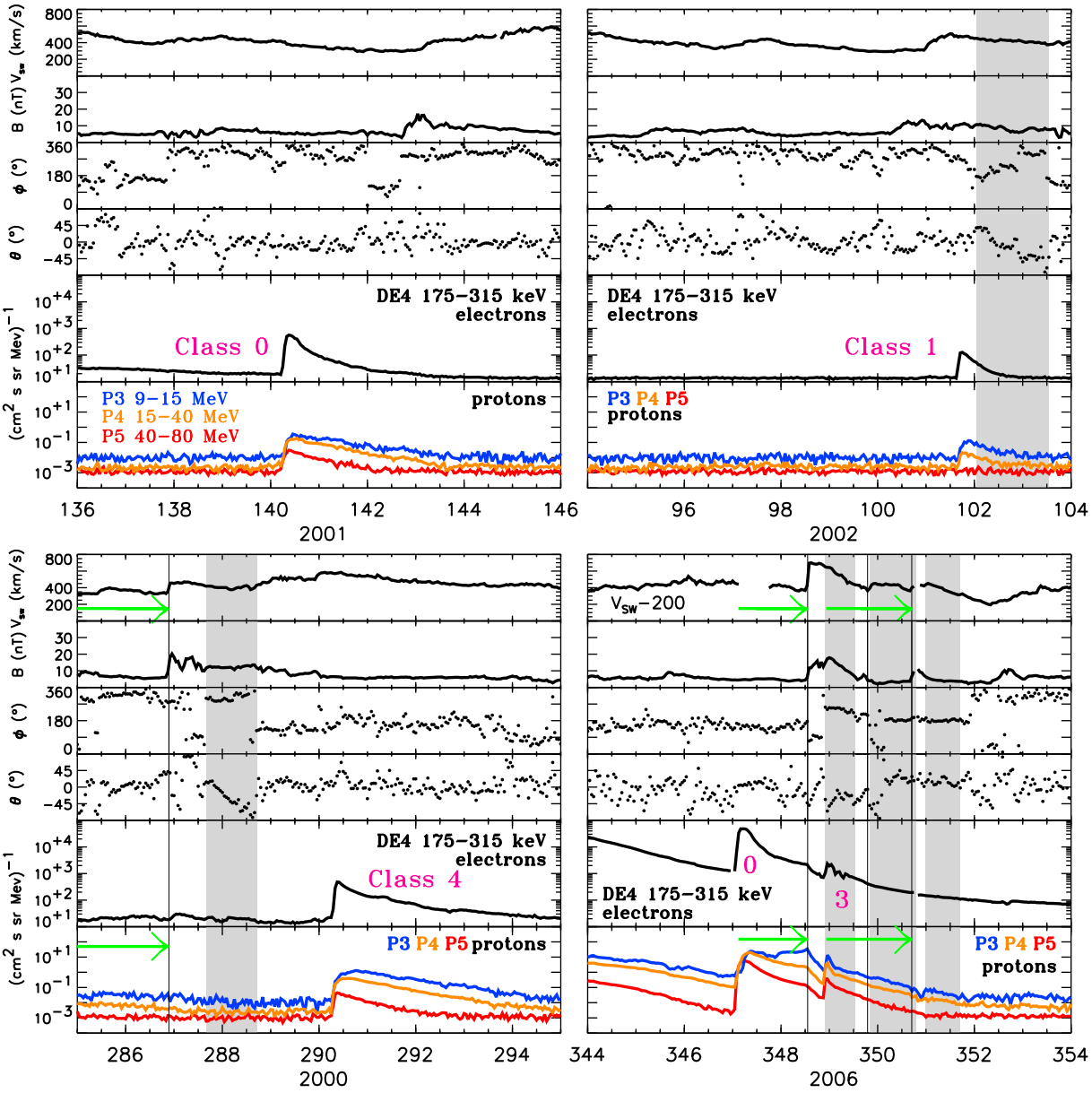


**Figure 2.** Examples of SEP events showing their classification according to the presence/absence of ICMEs in the IP medium. From top to bottom each panel shows hourly averages of the solar wind speed, magnetic field magnitude, magnetic field azimuth, and elevation angles in the RTN coordinate system, 175–315 keV electron intensities, and 9–15 MeV proton (P3, blue), 15–40 MeV proton (P4, orange) and 40–80 MeV proton (P5, red) intensities. The gray bars indicate the passage of ICMEs and the thin vertical solid lines the passage of IP shocks. The green horizontal arrows indicate, for those ICME that have an associated LASCO CME, the time spent by the CME-driven shocks to travel from Sun to 1 AU.

Figure 1 is a schematic representation of the IP environment assumed for each class of event. The large solid black dot in Figure 1 identifies the location of the observer at the time when the maximum intensity of the prompt component of the SEP events is observed. Although in our study the observer is always located near Earth at ~1 AU from the Sun, for illustration purposes, its location with respect to the presence of the ICME in the IP medium has been displaced in Figure 1.

A SEP event is classified as Class 0 when it is observed in absence of ICMEs. We have arbitrarily considered that no ICME is present during the development of a SEP event when no ICME is listed for a period of 72 h prior to and after the observation of the peak intensity in the prompt component of the event. Note that we exclude the observation of the ICME associated with the parent CME that generated the SEP event which usually occurs late in the event (i.e., well after the prompt component of the SEP event is measured) and

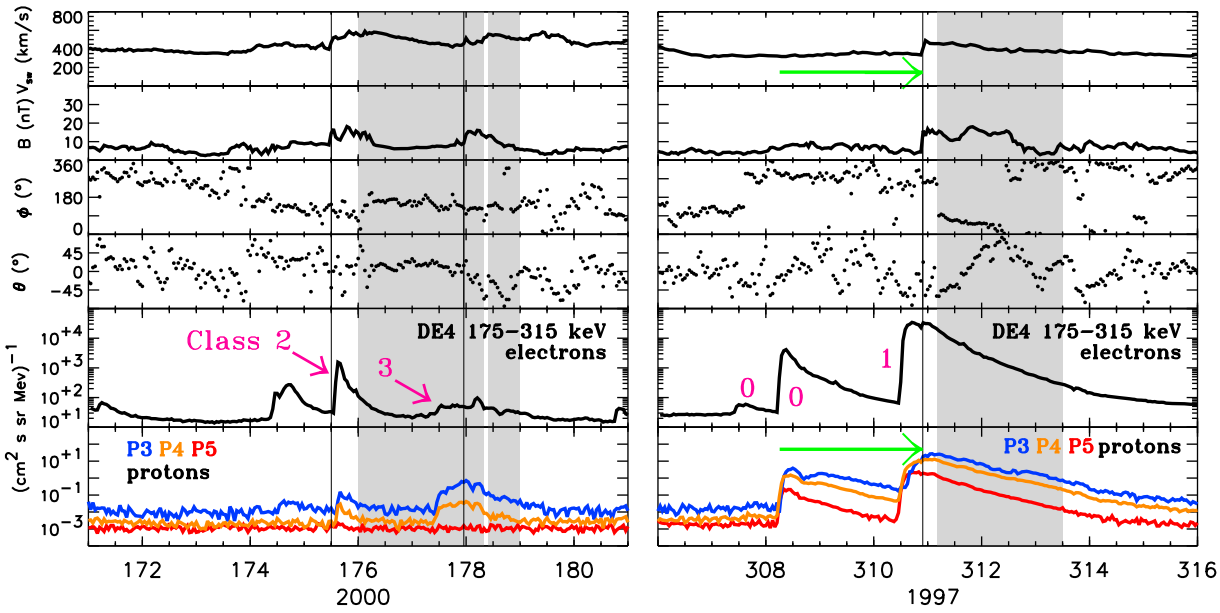


**Figure 3.** The same as Figure 2 for five additional SEP events listed in Table 1. The purple numbers indicate the class of the SEP events for the DE4 175–315 keV electron channel.

only in the case of events associated with Earth-directed CMEs. The assumption is that a Class 0 SEP event (Figure 1a) occurs under undisturbed solar wind conditions, i.e., without the presence of any preceding ICME either between the Sun and Earth or beyond Earth.

Class 1 events (Figure 1b) are those SEP events in which an ICME is present between the Sun and Earth at the time when the peak intensity of the prompt component of the SEP event is observed. In these events, the ICME arrives at Earth shortly after the maximum intensity of the SEP is observed and the ICME is not associated with the parent CME that originated the SEP event. Class 2 events (Figure 1c) are those SEP events in which the maximum particle intensity happens to occur between the passage of a preceding shock and the ICME that presumably was responsible for the origin of the shock previously observed. In other words, Class 2 events is when the peak intensity is observed in the sheath formed between the shock and the ICME of a preceding event. If the preceding ICME did not drive a shock, the SEP event is then classified as Class 1.

Class 3 events (Figure 1d) are those SEP events with peak intensities observed when Earth is immersed within a preceding ICME. Class 4 events (Figure 1e) are those SEP events observed after the passage of an ICME. We have arbitrarily considered an upper limit of 72 h between the passage of the rear edge of the preceding ICME and the observation of the peak intensity in the prompt component of the SEP event (an ICME moving at 600 km $s^{-1}$ would move ~1 AU in these 72 h). Finally, we added a Class 5 to include those SEP events in which ICMEs are observed before and after the peak intensity of the prompt component of the event and therefore multiple scenarios are possible. For those SEP events in which the peak intensity of the prompt component is observed when Earth is immersed in an ICME, but other ICMEs are observed before and after, we have prioritized the fact that the peak of the event occurs inside an ICME and classified the event as Class 3.

Figures 2 and 3 show several examples of SEP events in each group. Each panel shows, from top to bottom, solar wind speed, magnetic field magnitude, and magnetic field orientation in the RTN coordinate system, as measured by the ACE spacecraft, the 175–315 keV electron intensities measured by the ACE/EPAM DE4 electron channel and the proton intensities in the differential energy channels P3 (9–15 MeV), P4 (15–40 MeV), and P5 (40–80 MeV) of GOES/EPS. The vertical gray bars indicate the passage of ICMEs identified by Richardson and Cane and the thin solid vertical lines the passage of interplanetary shocks. For some of these ICMEs, Richardson and Cane identify their most probable solar origin as seen by LASCO. The green horizontal arrows in the solar wind and proton flux panels identify the time interval spent by the CME-driven shock to travel from Sun to ACE according to the identification made by Richardson and Cane. That allows

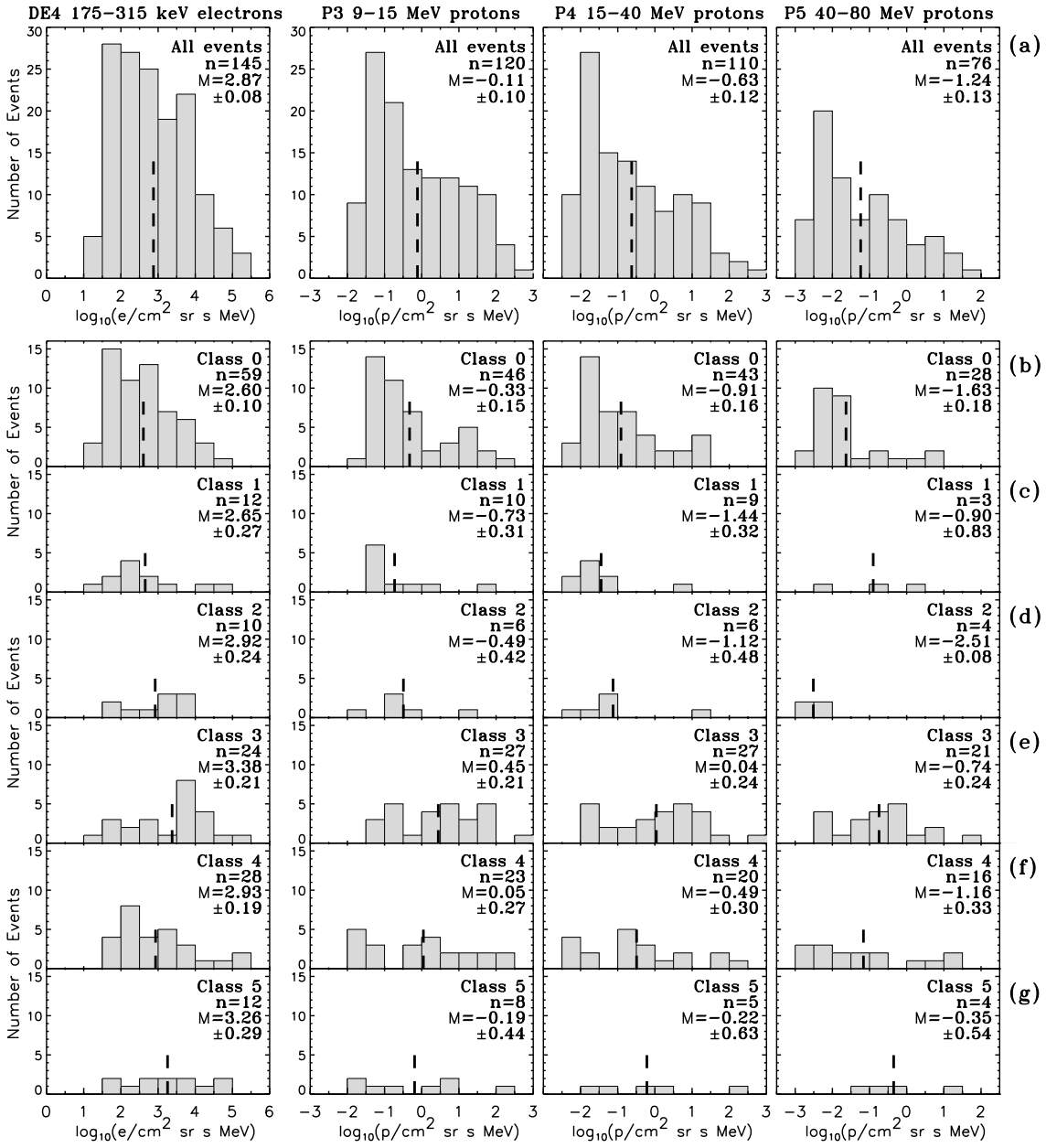


**Figure 4.** Distribution of the particle peak intensities for the different energy channels (from left to right DE4, P3, P4, and P5) and (a) for all the events regardless of their class association (top row) and (b–g) for the events in Classes 0, 1, 2, 3, 4 and 5 (from top to bottom). The dashed vertical line indicates the mean peak intensity *M*, and *n* the number of events in each distribution.

us to distinguish whether the observed ICME resulted from the CME at the Sun associated with the onset of the SEP event.

Figure 2 (top, left) shows the SEP event on day 140 of 2001 (event #64 in Table 1). This SEP event was observed under a relatively steady solar wind magnetic field without the presence of ICMEs before or after the event; therefore, we have classified this event as Class 0. Figure 2 (top, right) shows the event on day 101 of 2002 (event #82 in Table 1). Just a few hours after the peak of the event, an ICME without any clear parent coronagraph CME associated with it was observed early on day 102. The solar wind speed observed in this ICME implies that, at the time when the peak intensity of the event was observed, the ICME was located between the Sun and Earth; therefore, this ICME was an intervening structure for the SEPs, and we classify this event as Class 1. Figure 2 (bottom, left) shows the event on day 290 of 2000 (event #51 in Table 1) with

peak intensity observed 1.5 days after the passage of an ICME; therefore, this ICME was beyond Earth when the peak intensity was observed and we classify this event as Class 4.

Figure 2 (bottom, right) shows two SEP events with onsets early on day 347 and late on day 348 of 2006, respectively (events #146 and #147 in Table 1). No preceding ICME was observed before the first SEP event; therefore, we classify the event on day 347 as Class 0. The maximum intensity of the SEP event on day 348 was observed during the passage of an ICME (note that this ICME was the interplanetary counterpart of the CME associated with the origin of the SEP event #146 as indicated by the green horizontal arrow). Although the following ICME observed on day 350 acted as an intervening structure for the event on day 348, we prioritize the fact that the peak intensity occurred inside an ICME and classify this event as Class 3.

Figure 3 (left) shows two SEP events with onsets on day 175 and 177 of 2000 (note that the event with onset on day 174 was not included in the list of *Cane et al.* [2010], and therefore, it is not considered in our study). The peak intensity of the event on day 175 (event #42 in Table 1) occurred between the passage of an IP shock and an ICME, therefore, we classify this event as Class 2. The peak intensity of the prompt component of the SEP event with onset on day 177 (event #43 in Table 1) occurred within the passage of an ICME, therefore, we classify this event as Class 3.

Finally, Figure 3 (right) shows a sequence of three SEP events in November 1997. The first two events with onsets on days 307 and 308 (events #1 and #2) are Class 0 because no ICME was observed prior to or after the peak intensity of these events. The peak intensity of the event with onset on day 310 (event #3 in Table 1) was observed before the passage of the shock on day 310 in the energy channels DE4 and P5; however, the peak intensity in the energy channels P3 and P4 was observed in the sheath region of the following ICME (this ICME was the interplanetary counterpart of the CME that generated the SEP event with onset on day 308 as indicated by the green horizontal arrow). Since our classification of the events is based on the conditions at the time of the peak intensity, the class assigned to each event may depend on the selected energy channel. Therefore, the event on day 310 of 1997 is Class 1 for the channels DE4 and P5, but Class 2 for the energy channels P3 and P4.

Column 9 of Table 1 provides the classification of the SEP events according to the scheme above described. We list from left to right and separated by commas the class of the event for the DE4 (175–315 keV) electron channel, the P3 (9–15 MeV), P4 (15–40 MeV), and the P5 (40–80 MeV) proton channels. We have indicated by "–" when the event does not show any particle increase above the preevent background intensity in the corresponding energy channel and by "8" when the event does not show a peak intensity in its prompt component. For most of the events, the same Class applies to all energy channels, however, when the peak of the event is observed near the passage of a preceding ICME, different classes may apply to the different energy channels owing to the observation of the peak intensity on different side of the preceding IP structures. Note that we use 1 h resolution data for both particle peak intensity and ICME boundary identification. Slight differences in the event classification may appear when considering the use of higher time resolution data and the delay for the IP structures to travel from L1 to GOES. Column 10 of Table 1 lists the time where we have identified the maximum peak intensity in the 175–315 keV electron channel. Columns 11–14 provide the maximum intensity of the prompt component of the events in the DE4 175–315 keV electron channel, and the P3 9–15 MeV, P4 15–40 MeV, and P5 40–80 MeV proton channels, respectively. When the SEP event does not show a peak intensity in their prompt component, we have either neglected the event or indicated by −8.88E8 in Table 1 the energy channel where no peak intensity was identifiable.

Figure 4a (top row) shows the peak intensity distributions for all events listed in Table 1 for the energy channels DE4, P3, P4, and P5 (from left to right) regardless of their associated class. Figures 4b–4g show the distribution of the peak intensities for each energy channel (from left to right, DE4, P3, P4, and P5) and for the events, from top to bottom, in Classes 0, 1, 2, 3, 4, and 5. We have indicated in each panel the number of events $n$ and the mean value of the logarithms of the peak intensities $M$ together with their standard error. We note the low statistics in Classes 1, 2, and 5. The general trend is that the distributions of Class 0 events peak at low intensities, whereas the distributions of Class 3 and Class 4 events extend over a broad range of intensities with larger mean values than Class 0 events. The high-intensity events within Classes 3 and 4 contribute to extend the high-intensity tail in the distributions of all events (top row). The two-sample Kolmogorov-Smirnov test applied to the distribution of events Class 0 and Class 3 indicates that the probability that both distributions are drawn from a single parent distribution is less than 1%. The probability that the distributions of events in Class 0 and Class 4 are derived from the same parent distribution is less than

**Table 2.** Properties of the Primary and Preceding CMEs for the SEP Events Classified as P and NP* [a]

| Event # | Primary CME | | | | | | Preceding CME | | | | | |
|---|---|---|---|---|---|---|---|---|---|---|---|---|
| | Date | Time | PA | $W$ | $V_{CME}$ | Flare[b] | Date | Time | PA | $W$ | $V_{CME}$ | Flare[c] |
| (1) | (2) | (3) | (4) | (5) | (6) | (7) | (8) | (9) | (10) | (11) | (12) | (13) |
| 001 | 1997/11/3 | 11:11 | 233 | 122 | 0352 | S17° W022° | 1997/11/03 | 09:53 | 238 | 071 | 0338 | S20° W015° |
| 002 | 1997/11/4 | 06:10 | Halo | 360 | 0785 | S14° W033° | 1997/11/03 | 11:11 | 233 | 122 | 0352 | S17° W022° |
| 003 | 1997/11/6 | 12:11 | Halo | 360 | 1556 | S18° W063° | 1997/11/06 | 04:20 | 263 | 059 | 0307[d] | S15° W056° |
| 006 | 1998/4/20 | 10:07 | 284 | 243 | 1863 | S W090° | 1998/04/20 | 03:16 | 237 | 043 | 0316[d] | – |
| 007 | 1998/5/2 | 14:06 | Halo | 360 | 0938 | S15° W015° | 1998/05/02 | 05:32 | Halo | 360 | 0542 | S20° W007° |
| 008 | 1998/5/6 | 08:29 | 309 | 190 | 1099 | S11° W065° | 1998/05/06 | 00:02 | 274 | 110 | 0786 | S16° W060° |
| 015 | 1998/11/5 | 20:44 | Halo | 360 | 1118 | N26° W018° | 1998/11/05 | 02:03 | Halo | 360 | 0380 | N19° W013° |
| 024 | 1999/6/27 | 09:06 | 349 | 086 | 0903 | N22° W026° | 1999/06/26 | 19:54 | Halo | 360 | 0364 | – |
| 025 | 1999/8/28 | 18:26 | 120 | 245 | 0462 | S26° W014° | 1999/08/27 | 20:26 | 069 | 153 | 0769 | – |
| 026 | 1999/12/28 | 00:54 | 293 | 082 | 0672 | N20° W056° | 1999/12/27 | 12:30 | 292 | 061 | 0302 | N22° W042° |
| 027 | 2000/2/12 | 04:31 | Halo | 360 | 1107 | N26° W024° | 2000/02/11 | 21:08 | 277 | 173 | 0498 | N26° W020° |
| 029 | 2000/3/3 | 02:30 | 233 | 098 | 0841 | S15° W060° | 2000/03/02 | 13:54 | 235 | 076 | 0835 | S20° W058° |
| 035 | 2000/5/4 | 11:26 | 235 | >170 | 1404 | S20° W090° | 2000/05/04 | 04:50 | 239 | 062 | 1064 | S14° W090° |
| 041 | 2000/6/18 | 02:10 | 307 | 132 | 0629 | N23° W085° | 2000/06/17 | 04:40 | 293 | 098 | 0659 | N22° W072° |
| 042 | 2000/6/23 | 14:54 | 282 | >198 | 0847 | N23° W072° | 2000/06/23 | 05:54 | 311 | 078 | 0535 | N21° W069° |
| 048 | 2000/9/9 | 08:57 | 271 | 180 | 0554 | N07° W067° | 2000/09/09 | 01:59 | 282 | 112 | 0508 | N07° W060° |
| 049 | 2000/9/19 | 08:50 | 283 | 076 | 0766 | N14° W046° | 2000/09/18 | 23:50 | 268 | 120 | 0359 | N15° W038° |
| 050 | 2000/10/9 | 23:50 | Halo | 360 | 0798 | N01° W014° | 2000/10/09 | 14:06 | 262 | 193 | 0383 | N00° W017° |
| 052 | 2000/11/08 | 23:06 | 271 | >170 | 1738 | N10° W075° | 2000/11/08 | 17:06 | 252 | 042 | 0391[d] | N11° W079° |
| 054 | 2001/1/28 | 15:54 | Halo | 360 | 0916 | S04° W059° | 2001/01/28 | 09:30 | 270 | 079 | 0638 | – |
| 057 | 2001/3/29 | 10:26 | Halo | 360 | 0942 | N16° W012° | 2001/03/28 | 19:27 | 135 | 059 | 0258 | N14° W005° |
| 059 | 2001/4/2 | 22:06 | 261 | 244 | 2505 | N17° W072° | 2001/04/02 | 12:50 | 257 | 155 | 0731 | N15° W060° |
| 060 | 2001/4/12 | 10:31 | Halo | 360 | 1184 | S20° W042° | 2001/04/11 | 13:32 | Halo | 360 | 1103 | S22° W027° |
| 061 | 2001/4/14 | 17:54 | 263 | 113 | 0830 | S17° W071° | 2001/04/14 | 09:30 | 264 | 103 | 0310 | S18° W067° |
| 062 | 2001/4/15 | 14:06 | 245 | 167 | 1199 | S20° W084° | 2001/04/14 | 17:54 | 263 | 113 | 0830 | S16° W071° |
| 063 | 2001/4/26 | 12:30 | Halo | 360 | 1006 | N17° W031° | 2001/04/26 | 08:30 | 332 | 091 | 0740 | N24° W027° |
| 074 | 2001/10/19 | 01:27 | Halo | 360 | 0558 | N16° W018° | 2001/10/18 | 16:26 | 236 | 065 | 0325 | N16° W013° |
| 075 | 2001/10/19 | 16:50 | Halo | 360 | 0901 | N15° W029° | 2001/10/19 | 01:27 | Halo | 360 | 0558 | N16° W018° |
| 077 | 2001/11/4 | 16:35 | Halo | 360 | 1810 | N06° W018° | 2001/11/04 | 14:10 | 302 | 110 | 0844[d] | – |
| 078 | 2001/12/26 | 05:30 | 281 | >212 | 1446 | N08° W054° | 2001/12/26 | 02:06 | 283 | 021 | 0800[d] | – |
| 084 | 2002/4/15 | 03:06 | 308 | 055 | 0674 | N19° W079° | 2002/04/14 | 07:50 | 323 | 076 | 0757 | N19° W057° |
| 087 | 2002/5/22 | 03:50 | Halo | 360 | 1557 | S22° W053° | 2002/05/22 | 00:06 | 230 | 186 | 1246 | – |
| 091 | 2002/8/5 | 07:32 | 273 | 043 | 0689 | S07° W045° | 2002/08/04 | 21:30 | 251 | 083 | 0816 | – |
| 093 | 2002/8/16 | 06:06 | 293 | 162 | 1378 | N06° W083° | 2002/08/15 | 22:30 | 301 | 068 | 0857 | – |
| 095 | 2002/8/19 | 11:06 | 221 | 102 | 0549 | S12° W025° | 2002/08/18 | 21:54 | 203 | 140 | 0682 | S12° W019° |
| 096 | 2002/8/20 | 08:54 | 237 | >122 | 1099 | S10° W038° | 2002/08/20 | 01:54 | 244 | 157 | 0961 | S11° W035° |
| 097 | 2002/8/22 | 02:06 | Halo | 360 | 0998 | S07° W062° | 2002/08/21 | 03:54 | 248 | 077 | 0474 | S11° W047° |
| 098 | 2002/8/24 | 01:27 | Halo | 360 | 1913 | S02° W081° | 2002/08/23 | 13:27 | 286 | 103 | 0321 | S07° W082° |
| 101 | 2002/11/9 | 13:32 | Halo | 360 | 1838 | S12° W029° | 2002/11/08 | 18:30 | 196 | 062 | 0840 | S12° W019° |
| 103 | 2003/3/18 | 13:54 | Halo | 360 | 1042 | S09° W046° | 2003/03/18 | 12:30 | 263 | 209 | 1601 | S15° W046° |
| 104 | 2003/4/7 | 09:50 | 272 | 069 | 0719 | S10° W088° | 2003/04/07 | 03:50 | 273 | 095 | 0217 | – |
| 105 | 2003/4/23 | 01:27 | 271 | 248 | 0916 | N22° W025° | 2003/04/22 | 21:04 | 349 | 064 | 0369 | N20° W014° |
| 106 | 2003/4/24 | 13:27 | 317 | 242 | 0609 | N21° W039° | 2003/04/23 | 16:50 | 343 | 105 | 0596 | N20° W022° |
| 107 | 2003/5/28 | 00:50 | Halo | 360 | 1366 | S06° W020° | 2003/05/27 | 23:50 | Halo | 360 | 0964 | S07° W017° |
| 111 | 2003/10/26 | 17:54 | 270 | >171 | 1537 | N02° W038° | 2003/10/26 | 05:30 | 267 | 086 | 0684 | – |
| 112 | 2003/11/2 | 17:30 | Halo | 360 | 2598 | S14° W056° | 2003/11/01 | 23:07 | 254 | 093 | 0899 | S12° W060° |
| 113 | 2003/11/4 | 19:54 | Halo | 360 | 2657 | S19° W083° | 2003/11/04 | 12:54 | 263 | 072 | 0605 | – |
| 115 | 2003/11/20 | 08:06 | Halo | 360 | 0669 | N03° W012° | 2003/11/20 | 02:50 | 221 | 063 | 0364 | N03° W008° |
| 121 | 2004/7/25 | 14:54 | Halo | 360 | 1333 | N04° W033° | 2004/07/24 | 23:54 | 217 | 078 | 0555 | N03° W026° |
| 124 | 2004/10/30 | 06:54 | Halo | 360 | 0422 | N13° W022° | 2004/10/30 | 03:54 | 321 | 060 | 0138 | N13° W020° |
| 125 | 2004/10/30 | 12:30 | Halo | 360 | 0427 | N12° W026° | 2004/10/30 | 09:54 | 265 | 074 | 0552 | N14° W024° |
| 126 | 2004/10/30 | 16:54 | Halo | 360 | 0690 | N13° W028° | 2004/10/30 | 12:30 | Halo | 360 | 0427 | N12° W026° |
| 127 | 2004/11/7 | 16:54 | Halo | 360 | 1759 | N09° W017° | 2004/11/07 | 14:30 | 286 | 100 | 0226 | N08° W014° |
| 129 | 2004/11/10 | 02:26 | Halo | 360 | 2000 | N09° W049° | 2004/11/09 | 17:26 | Halo | 360 | 2000 | N07° W051° |
| 130 | 2005/1/17 | 09:54 | Halo | 360 | 2547 | N15° W025° | 2005/01/17 | 09:30 | Halo | 360 | 2094 | N13° W023° |
| 131 | 2005/1/20 | 06:54 | Halo | 360 | 2500 | N14° W061° | 2005/01/19 | 08:30 | Halo | 360 | 2020 | N15° W051° |
| 132 | 2005/5/6 | 03:30 | 280 | 109 | 1120 | S04° W071° | 2005/05/05 | 20:30 | Halo | 360 | 1180 | S04° W067° |
| 133 | 2005/5/6 | 11:54 | 277 | 129 | 1144 | S04° W076° | 2005/05/06 | 03:30 | 280 | 109 | 1120 | S04° W071° |
| 134 | 2005/5/11 | 20:13 | Halo | 360 | 0550 | S10° W055° | 2005/05/11 | 07:32 | 236 | 095 | 0305 | S11° W045° |
| 139 | 2005/7/12 | 16:54 | Halo | 360 | 0523 | N11° W067° | 2005/07/11 | 17:30 | 275 | 069 | 0462 | N14° W056° |

**Table 2.** (continued).

| Event # | Primary CME | | | | | | Preceding CME | | | | | |
|---|---|---|---|---|---|---|---|---|---|---|---|---|
| | Date | Time | PA | $W$ | $V_{CME}$ | Flare[b] | Date | Time | PA | $W$ | $V_{CME}$ | Flare[c] |
| (1) | (2) | (3) | (4) | (5) | (6) | (7) | (8) | (9) | (10) | (11) | (12) | (13) |
| 140 | 2005/7/13 | 03:06 | 288 | 054 | 0759 | N18° W082° | 2005/07/12 | 16:54 | Halo | 360 | 0523 | N11° W064° |
| 141 | 2005/7/13 | 14:30 | Halo | 360 | 1423 | N11° W078° | 2005/07/12 | 16:54 | Halo | 360 | 0523 | N11° W067° |
| 142 | 2005/7/14 | 10:54 | Halo | 360 | 2115 | N08° W089° | 2005/07/14 | 07:54 | 266 | 103 | 0752 | N11° W073° |
| 143 | 2005/8/22 | 01:32 | Halo | 360 | 1194 | S09° W048° | 2005/08/21 | 12:06 | 267 | 061 | 0287 | S09° W042° |
| 144 | 2005/8/22 | 17:30 | Halo | 360 | 2378 | S12° W060° | 2005/08/22 | 01:32 | Halo | 360 | 1194 | S11°W054° |
| 145 | 2006/7/6 | 08:54 | Halo | 360 | 0911 | S11° W032° | 2006/07/06 | 01:32 | 219 | 110 | 0250 | – |
| 146 | 2006/12/13 | 02:54 | Halo | 360 | 1774 | S06° W023° | 2006/12/12 | 20:28 | 193 | 050 | 0474[d] | – |
| 147 | 2006/12/14 | 22:30 | Halo | 360 | 1042 | S07° W046° | 2006/12/14 | 20:30 | 237 | 016 | 0316[d] | – |

[a]As listed in cdaw.gsfc.nasa.gov/CME_list where Time indicates the first observation time of the CME in LASCO images on the indicated day, PA is the position angle (in degrees), W is the CME width (in degrees) and $V_{CME}$ the plane-of-sky speed (in km $s^{-1}$). Note that the properties of the preceding CME for event on day 111 of 2002 classified as NP* [or Other by *Gopalswamy et al.*, 2004] do not exist. Dates are formatted as year/month/day.

[b]Flare location as listed in Table 1 of *Cane et al.* [2010].

[c]Flare location based on either the occurrence of a solar flare listed in www.swpc.noaa.gov or the observation of an EIT eruption.

[d]For some of the most intense SEP events, *Ding et al.* [2013] identified a < 60° CME preceding the primary CME.

30% for energy channels P3 and P4, 48% for P5 and 66% for DE4. We conclude that significant differences exist between the peak intensity distributions of Class 0 and Class 3 events, whereas for Class 4 these differences are more significant in Channels P3 and P4 than in P5 and DE4. For the other classes, the uncertainties associated with the low statistics of each group do not allow us to draw firm conclusions.

### 2.2. SEP Event Classification Based on Coronagraph CME Observations

The use of near-Earth in situ ICME observations to determine the properties of the interplanetary medium where SEPs propagate is very limited, especially for those events classified as Class 1 for which we inferred the presence of an ICME located between the Sun and the observer. Figure 5 of *Richardson and Cane* [2010] shows that ICMEs detected at Earth can originate from longitudes ranging from E50° to W50° with a clear predominance of CMEs launched from longitudes close to the Sun-Earth line (64% of ICMEs observed near Earth originate from a range of longitudes ±20° from central meridian). The prompt observation of SEPs requires the injection of particles onto a field line connecting with the observer which usually resides at the west of the Sun-Earth line (~W60° for slow solar wind conditions). For SEP events in Classes 2 and 4, we can be certain that the observation of an ICME or a shock prior to the peak intensity of the SEP event implies that such IP structures were located beyond Earth at the time when the bulk of SEPs reached the observer, and that most likely these structures, because of their angular extent, might have had a real effect in reflecting SEPs back to the observer. For SEP events in Class 3, we can also be certain that the in situ observation of an ICME during the maximum of the SEP event implies that the bulk of particles propagated within the ICME to reach the observer and that most likely their transport was controlled by such structure. However, for SEP events in Class 1, the observation of a preceding ICME after the onset of the SEP event does not imply that the transport of SEPs has been affected by the presence of this ICME. For example, it is easy to envision the launch of a preceding CME from an active region in a longitude close to the Sun-Earth line followed by the occurrence of a western flare from an unrelated active region located close to the root of the IMF line connecting the observer with the Sun. Depending on the time elapsed between the launch of the preceding CME and the injection of SEPs by the primary CME, it is possible that the SEP propagation toward the observer is not affected by the preceding CME. For this reason, we have added an alternative criterion to determine whether a preceding ICME was present between the Sun and Earth when the injection of SEPs from the primary CME took place.

In order to identify whether an ICME was present in IP space before the occurrence of the main CME and that most likely this preceding ICME affected the transport of the SEPs injected at the time of the primary CME, we have applied the same criteria used by *Gopalswamy et al.* [2004]. We have searched for preceding CMEs ejected from the same source region as the primary CMEs satisfying the following two criteria: (1) the preceding CME should have been launched within 24 h ahead of the onset time of the primary CME and (2) the preceding CME must be wider than 60°.

The selection of 24 h as a time window to determine the precedence of a CME comprises a wide range of heliocentric distances where the preceding CME might have been located at the time of the SEP injection,

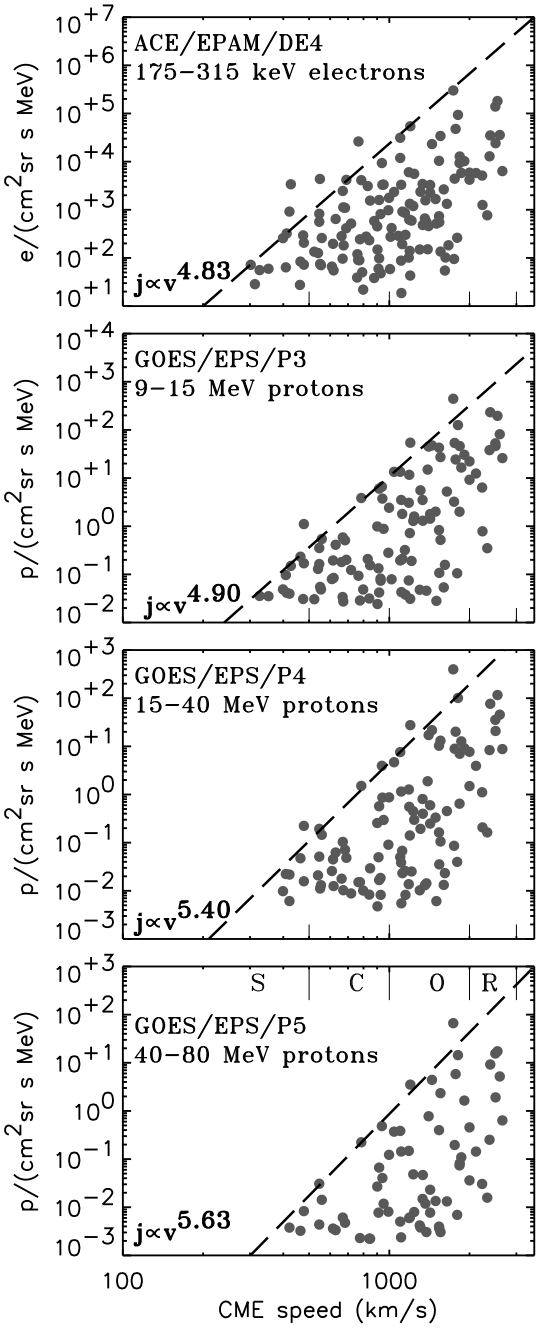


**Figure 5.** SEP peak intensities versus sky-plane speed of the associated primary CMEs. The dashed straight lines ($j \propto v^{\alpha}$) are visual indications of the upper limit of the SEP peak intensities. The letters S, C, O, and R indicate the type of CME according to the scheme proposed by *Evans et al.* [2013].

but mostly within 1 AU and thus located between the Sun and Earth. For example, a preceding CME moving at 400 km $s^{-1}$ would be located at ~0.23 AU from the Sun in these 24 h whereas a preceding CME at 1500 km $s^{-1}$ would be at ~0.87 AU. For shorter elapsed times between the preceding and the primary CMEs, the preceding CME will be closer to the Sun at the time when the primary CME is ejected.

The condition that the preceding CME originates from the same active region as the primary CME implies that SEPs injected at the time of the primary CME must propagate through field lines distorted by the preceding CME. The condition that the preceding CME must be wider than >60° increases the probability that a wide region of the interplanetary medium was affected. The use of wide CMEs also responds to the technical difficulty of detecting narrow CMEs from close to the disk center using coronagraph observations.

We have based our study on the catalog of CMEs observed by LASCO posted on cdaw.gsfc.nasa.gov/CME_list/ and described in *Yashiro et al.* [2004]. The identification of the solar origin of the preceding CMEs was based on either prior reports [e.g., *Gopalswamy et al.*, 2004; *Ding et al.*, 2013] or inspection of images from the Extreme-ultraviolet Imaging Telescope (EIT) on board SOHO. Owing to the uncertainties in the origin of the events occurring behind the limb, we have classified only those events with identifiable origin on the visible side of the Sun (as seen from Earth). We have indicated in Column 15 of Table 1 whether a preceding CME fulfilling the above criteria was identified in the catalog (P) or not (NP). For a few events, a CME fulfilling the criteria of width and time, and moving the same direction as the primary CME, was observed but we could not identify its origin (indicated by Y in Column 15 of Table 1). A few events with data limitations (indicated by dg in Column 15 of Table 1) did not allow us to determine if a preceding CME was present. Out of the 147 SEP events of Table 1, 126 events were associated with solar activity in the visible solar disk, 11 occurred during LASCO data gaps, two events were classified as Y, 61 as P, and 52 as NP. Among the most intense SEP events classified as NP, we distinguish also those that either *Ding et al.* [2013] identified the occurrence of a preceding CME not listed in the CDAW catalog, or *Gopalswamy et al.* [2004] identified the occurrence of a preceding eruption not registered in the LASCO catalog of CMEs because the primary CME followed so closely that it overtook the preceding CME within the occulting disk of LASCO. These latter SEP events are part of the group classified as "Other" by *Gopalswamy et al.* [2004]. We indicate in column 15 of Table 1 a total of eight events by NP* (where * indicates this particularity described in the

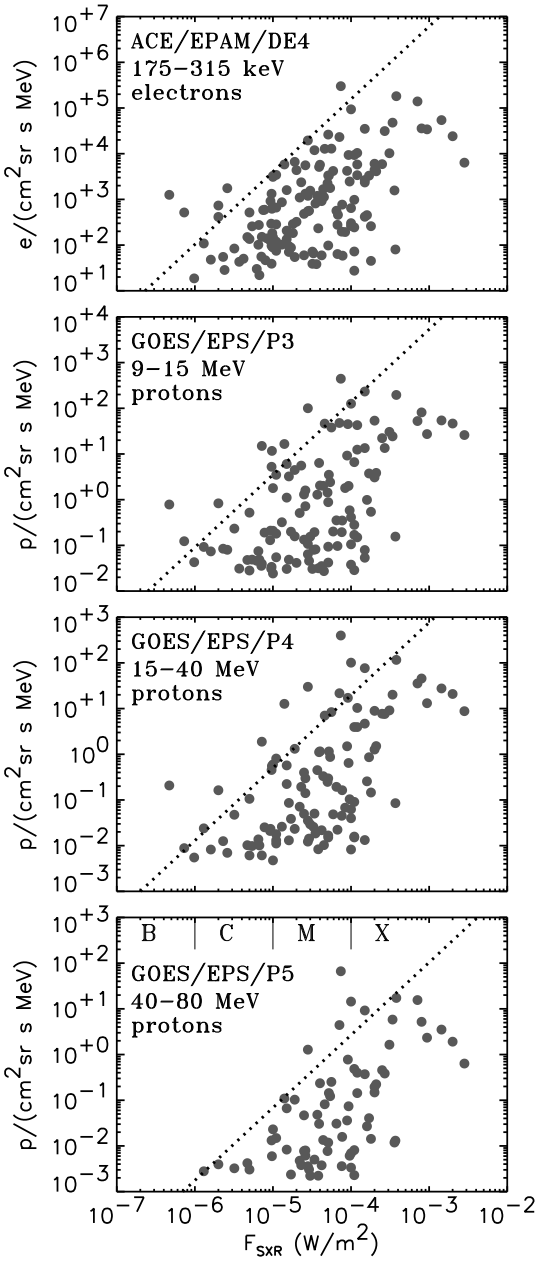


**Figure 6.** SEP peak intensities versus the soft X-ray solar flare peak flux. The dashed straight lines follow a law $j \propto (F_{SXR})^{1.59}$ inferred by *Cliver et al.* [2012].

footnotes of Table 1). Note that Column 15 of Table 1 does not constitute a complete list of this type of events since we have only indicated this possibility for the most intense SEP events where a preceding ICME was not listed in the CDAW catalog but other works identified some preceding activity.

Table 2 lists the properties of the primary and the preceding CMEs for those events classified as P or NP* in Table 1. Column 1 of Table 2 lists the event number as listed in Column 1 of Table 1. Columns 2–6 of Table 2 give the characteristics of the primary CME, including the date and first observing time, its position angle (PA) measured counterclockwise in the plane of sky from Solar North (in degrees), the angular width of the CME (W) and the CME speed ($V_{CME}$) estimated from linear time-position fits. Column 7 of Table 2 determines the location of the flare site associated with the primary CME. Both CME parameters and flare associations are based on Table 1 of *Cane et al.* [2010] and have been checked with the catalog of LASCO CMEs at cdaw.gsfc.nasa.gov/CME_list/. Columns 8–13 give the same parameters for the preceding CME. Note that if there were more than one preceding CME satisfying the above criteria, Table 2 lists the CME closest in time to the primary CME.

## 3. Relationship Between SEP Peak Intensities, CME Speed Type and Soft X-ray Flare Class

Figure 5 shows the SEP peak intensities listed in columns 11–14 of Table 1 versus the plane-of-sky speeds of the associated CMEs (listed in column 8 of Table 1). We have indicated in Figure 5 (bottom) the type of the CME according to the SCORE Scale proposed by *Evans et al.* [2013] based on the plane-of-sky CME speed (S for slow CMEs with speeds less than 500 km $s^{-1}$, C for common CMEs with speeds between 500 and 999 km $s^{-1}$, O for occasional CMEs with speeds between 1000 and 1999 km $s^{-1}$, and R for rare CMEs with speeds between 2000 and 2999 km $s^{-1}$). The most common CME type associated with the selected SEP events is the O type. Figure 5 shows that the peak intensity versus the CME speed follows, in a good approximation, a triangular distribution. Prior attempts to find correlations between the logarithms of the SEP peak intensities and the logarithms of the CME speeds have indicated the large spread of peak intensities over several orders of magnitude for similar values of CME speeds [e.g., *Kahler*, 2001]. For a given CME speed, the range in associated SEP peak intensities extends over 3 or 4 orders of magnitude, making a possible prediction of peak intensities virtually impossible. Rather than trying to find a correlation between SEP peak intensity and CME speed (see, for example, *Gopalswamy et al.* [2004] and *Miteva et al.* [2013] for a discussion of the quality of correlations for different types or classes of events), we consider more appropriate the use of these triangular distributions as a method to provide upper limits to the particle intensity that can be observed in

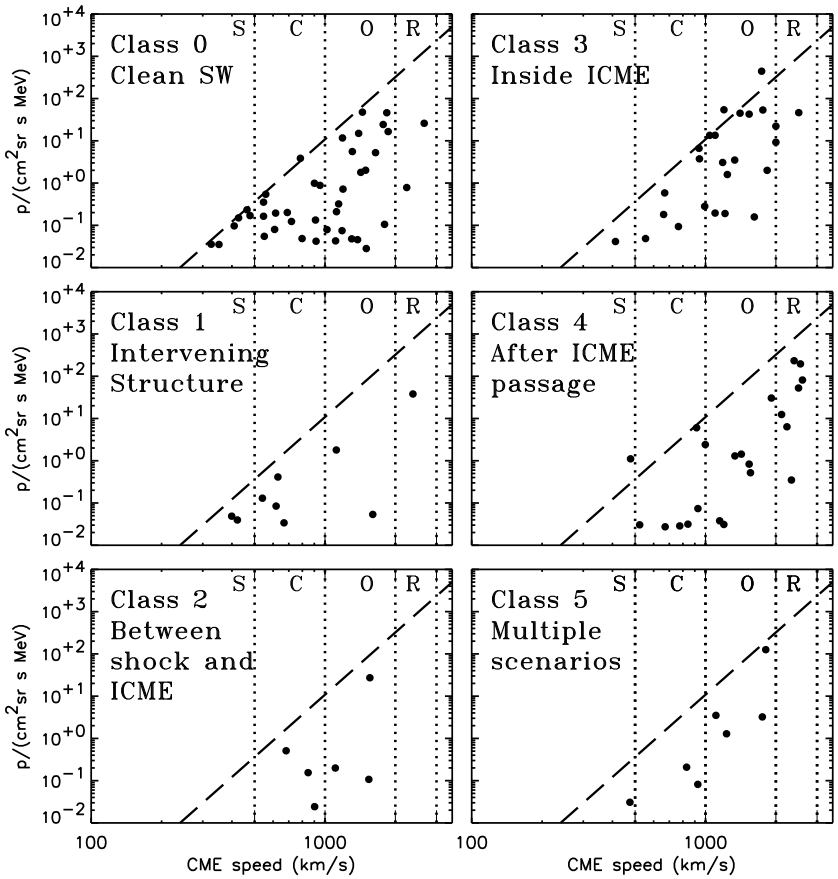


**Figure 7.** The 9–15 MeV proton peak intensities versus sky-plane speed of the associated primary CME distinguishing the events in each class according to the presence/absence of ICMEs. The dotted vertical lines and the letters S, C, O, and R indicate the type of associated CME according to their sky-plane speed. The dashed lines indicate the slope $j \propto v^{4.90}$ plotted in the panel P3 9–15 MeV proton channel of Figure 5.

the prompt component of the SEP events. The dashed straight lines in each panel of Figure 5 provide, for a given CME speed and with the exception of a few events (see below), the upper limit of peak intensity to be observed in the prompt component of the associated SEP event.

The empty upper left triangles in the different panels of Figure 5 indicate that the most intense SEP events are associated with the fastest CMEs. On the other hand, Figure 5 also shows an empty lower right corner in the distributions indicating that the fastest CMEs do not produce low intensity SEP events. In other words, the type R CMEs are most likely to produce intense SEP events. *Gopalswamy et al.* [2008a] found that for western CMEs, the SEP association rate increases linearly from ~30% for 800 km $s^{-1}$ to 100% for >1800 km $s^{-1}$. However, it is worthwhile to indicate that some narrow fast CMEs have not been associated with SEP particle enhancements [e.g., *Kahler and Reames*, 2003; *Gopalswamy et al.*, 2008b].

Figure 6 shows the scatter plot of SEP peak intensities versus the associated flare soft X-ray peak 1–8 Å flux ($F_{SXR}$). Dependence between $F_{SXR}$ and SEP peak intensities have been previously found with discreet correlation coefficients [e.g., *Gopalswamy et al.*, 2003; *Garcia*, 2004; *Park et al.*, 2010; *Cliver et al.*, 2012; *Miteva et al.*, 2013]. Although it is always possible to find a sufficiently high upper limit to the peak intensities of the SEP events, it is clear that such distributions are not so clearly defined as the distributions shown in Figure 5. The dotted lines in Figure 6 follow a law $j \propto (F_{SXR})^{1.59}$ that is the linear regression obtained by *Cliver et al.* [2012] using 58 >10 MeV proton SEP events but slid in both directions to determine a possible upper limit for the peak intensities as done in Figure 5. The largest peak intensity was associated with a M7.4 flare (event #52 on 2000/11/8), and there is a trend for the peak intensity distributions to flatten for flare classes above X10.

**Table 3.** Peak Intensity Averages for Each Energy Channel and Class of SEP Event[a]

| Energy Channel | CME | | | | Flare | | | All Events[b] |
|---|---|---|---|---|---|---|---|---|
| | S | C | O | R | C | M | X | |
| DE4 all events | 1.40E2 (14) | 3.83E2 (48) | 1.27E3 (60) | 1.30E4 (11) | 1.53E2 (33) | 7.86E2 (72) | 3.23E3 (36) | 7.51E2 (145) |
| DE4 Class 0 (clean) | 1.26E2 (9) | 2.80E2 (18) | 7.43E2 (25) | 1.26E3 (1) | 1.98E2 (14) | 5.50E2 (29) | 4.63E2 (12) | 4.02E2 (59) |
| DE4 Class 1 (inter) | 2.57E2 (1) | 1.44E2 (4) | 1.10E3 (5) | 1.29E4 (1) | 9.49E0 (6) | 1.18E3 (3) | 3.88E3 (3) | 4.50E2 (12) |
| DE4 Class 2 (sheath) | – (0) | 7.18E2 (6) | 1.04E3 (4) | – (0) | 5.03E1 (1) | 9.62E2 (8) | 4.42E3 (1) | 8.34E2 (10) |
| DE4 Class 3 (inside) | 9.60E1 (2) | 1.05E3 (7) | 3.86E3 (11) | 2.90E4 (2) | 2.85E1 (1) | 1.80E3 (13) | 5.38E3 (10) | 2.39E3 (24) |
| DE4 Class 4 (after) | 2.07E2 (1) | 2.63E2 (11) | 5.42E2 (7) | 1.44E4 (7) | 1.54E2 (9) | 6.17E2 (12) | 1.35E4 (7) | 8.55E2 (28) |
| DE4 Class 5 (multi) | 2.94E2 (1) | 1.59E3 (2) | 3.76E3 (8) | – (0) | 4.18E2 (2) | 7.45E2 (7) | 3.75e4 (3) | 1.80E3 (12) |
| P3 all events | 8.63E−2 (11) | 1.97E−1 (37) | 1.85E0 (52) | 1.99E1 (11) | 1.47E−1 (24) | 6.59E−1 (59) | 4.84E0 (48) | 7.69E−1 (120) |
| P3 Class 0 (clean) | 9.47E−2 (6) | 2.19E−1 (14) | 1.01E0 (20) | 4.51E0 (2) | 2.76E−1 (11) | 6.24E−1 (21) | 7.30E−1 (10) | 4.72E−1 (46) |
| P3 Class 1 (inter) | 4.40E−2 (2) | 1.11E−1 (4) | 3.10E−1 (2) | 3.80E1 (1) | 5.66E−2 (6) | 8.26E0 (2) | 1.49E0 (2) | 1.86E−1 (10) |
| P3 Class 2 (sheath) | – (0) | 1.24E−1 (3) | 8.35E−1 (3) | – (0) | – (0) | 1.32E−1 (5) | 2.73E1 (1) | 3.22E−1 (6) |
| P3 Class 3 (inside) | 4.14E−2 (1) | 4.43E−1 (7) | 6.75E0 (16) | 4.64E1 (1) | 1.90E−1 (1) | 1.18E−1 (15) | 1.16E1 (11) | 2.79E0 (27) |
| P3 Class 4 (after) | 1.11E0 (1) | 1.35E−1 (7) | 6.02E−1 (7) | 2.45E1 (7) | 1.51E−1 (5) | 5.30E−1 (10) | 9.73E0 (8) | 1.11E0 (23) |
| P3 Class 5 (multi) | 3.08E−2 (1) | 1.30E−1 (2) | 6.54E0 (4) | – (0) | 3.08E−2 (1) | 4.43E−1 (6) | 1.26E2 (1) | 6.43E−1 (8) |
| P4 all events | 2.42E−2 (7) | 5.13E−2 (34) | 4.42E−1 (51) | 7.33E0 (11) | 3.21E−2 (19) | 1.74E−1 (56) | 1.86E0 (31) | 2.37E−1 (110) |
| P4 Class 0 (clean) | 2.45E−2 (4) | 5.99E−2 (14) | 2.12E−1 (19) | 1.35E0 (2) | 5.05E−2 (10) | 1.60E−1 (21) | 3.89E−1 (8) | 1.22E−1 (43) |
| P4 Class 1 (inter) | 7.75E−3 (2) | 2.54E−2 (3) | 2.27E−2 (3) | 8.36E0 (1) | 1.12E−2 (4) | 1.95E−1 (3) | 2.88E−2 (2) | 3.58E−2 (9) |
| P4 Class 2 (sheath) | – (0) | 2.15E−2 (3) | 2.61E−1 (3) | – (0) | – (0) | 2.67E−2 (5) | 1.31E1 (1) | 7.49E−2 (6) |
| P4 Class 3 (inside) | – (0) | 1.02E−1 (7) | 1.94E0 (16) | 4.00E1 (2) | 2.52E−2 (1) | 3.73E−1 (14) | 5.25E0 (12) | 1.09E0 (27) |
| P4 Class 4 (after) | 2.23E−2 (1) | 4.18E−2 (6) | 2.24E−1 (6) | 7.15E0 (6) | 3.15E−2 (4) | 1.77E−1 (9) | 2.62E0 (7) | 3.22E−1 (20) |
| P4 Class 5 (multi) | – (0) | 1.85E−2 (1) | 1.46E0 (4) | – (0) | – (0) | 1.69E−1 (4) | 1.01E2 (1) | 6.08E−1 (5) |
| P5 all events | 4.66E−3 (3) | 1.39E−2 (19) | 6.87E−2 (39) | 8.78E−1 (10) | 4.48E−3 (7) | 2.95E−2 (39) | 2.88E−1 (29) | 5.77E−2 (76) |
| P5 Class 0 (clean) | 3.49E−3 (2) | 1.58E−2 (8) | 2.74E−2 (14) | 6.35E−1 (1) | 4.95E−3 (5) | 2.52E−2 (14) | 6.56E−2 (8) | 2.33E−2 (28) |
| P5 Class 1 (inter) | – (0) | 3.35E−3 (1) | 2.34E0 (1) | 2.52E−1 (1) | – (0) | 2.52E−1 (1) | 8.85E−2 (2) | 1.25E−1 (3) |
| P5 Class 2 (sheath) | – (0) | 3.25E−3 (2) | 2.92E−3 (2) | – (0) | – (0) | 3.08E−3 (4) | – (0) | 3.08E−3 (4) |
| P5 Class 3 (inside) | – (0) | 3.14E−2 (4) | 1.94E−1 (13) | 4.20E0 (2) | – (0) | 8.10E−2 (10) | 3.71E−1 (11) | 1.80E−1 (21) |
| P5 Class 4 (after) | 8.31E−3 (1) | 1.43E−2 (4) | 2.35E−2 (5) | 6.77E−1 (6) | 3.47E−3 (2) | 2.01E−2 (8) | 9.54E−1 (6) | 6.86E−2 (16) |
| P5 Class 5 (multi) | – (0) | – (0) | 4.47E−1 (4) | – (0) | – (0) | 8.32E−2 (2) | 2.40E0 (2) | 4.47E−1 (4) |

[a]Averages computed using the logarithm of the peak intensities in each CME speed type (S, C, O, and R) and each soft X-ray flare class (C, M, and X) for the energy channels DE4 (175–315 keV electrons), P3 (9–15 MeV protons), P4 (15–40 MeV protons) and P5 (40–80 MeV protons).
[b]Regardless of the type of CME or X-ray flare class associated with.

## 4. Peak Intensity Averages

Figure 7 shows the proton peak intensity measured in channel P3 (9–15 MeV) as a function of the CME speed for each class of event following the scheme described in section 2.1 to identify the presence or absence of ICMEs. The dashed straight lines are the same as shown for this energy in Figure 5 (e.g., $j \propto v^{4.90}$). With the exception of Class 0, the rest of the classes include events occurring in a disturbed IP medium. Note that the few events above the dashed straight lines correspond to events in Classes 3 and 4. It is well known that most of the fastest CMEs usually occur in series [*Ruzmaikin et al.*, 2011]. Therefore, it is not surprising that most of the events associated with R-type CMEs are in Class 4 and that only 25% of the events associated with CMEs of speeds >1500 km $s^{-1}$ are Class 0. Similarly, the most intense events with P3 peak intensity above $10^2$ protons $(cm^2\ s\ sr\ MeV)^{-1}$ occur only in Classes 3, 4, and 5. On the other hand, there is a general lack of intense events in Class 1, with only one event above $10^1$ protons $(cm^2\ s\ sr\ MeV)^{-1}$ or two events above $10^0$ protons $(cm^2\ s\ sr\ MeV)^{-1}$.

For each type of the associated CME (S, C, O, and R) we have computed the number of events in each class and the average of the logarithms of their peak intensities. Table 3 lists, for each energy channel and each class of event, both the number of events (in parentheses) and the average of the logarithms of the peak intensities, observed in each CME speed type and each X-ray flare class. The limited number of events in some of these subgroups implies that comparisons of the averaged peak intensities of events associated with CMEs of similar speed or flares in the same X-ray class should be cautiously considered because of both poor statistics and the weight that the most intense SEP events have in computing the averaged peak intensity. The most populated classes of events associated with CMEs of similar speed are Class 3 and Class 0 associated with O-type CMEs. With the exception of events associated with S-type CMEs and C-class flares (where the number of Class 3 events is very low), Class 3 events always show, on average, higher peak

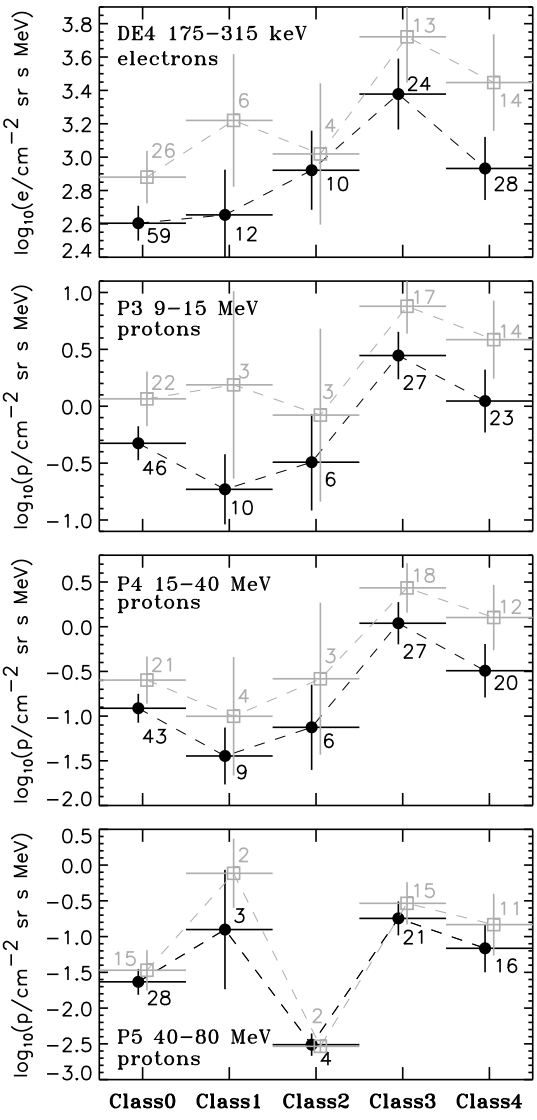


**Figure 8.** Average values of the peak intensities of the prompt component of the SEP events (black symbols) regardless of the associated CME speed or X-ray flare class and (gray symbols) associated with CMEs of speed >1000 km $s^{-1}$, for SEP events of Classes 0 to 4 (from left to right) and the energy channels (from top to bottom) DE4, P3, P4, and P5. The numbers indicate the number of events in each class. The vertical bars indicate the standard errors obtained from the average of the logarithms of the peak intensities.

intensities than those of Class 0. For the rest of the classes, the number of events in each group should be carefully examined before comparison.

The last column of Table 3 shows the total number of events for which we were able to determine a peak intensity in their prompt component in each event class and for each energy channel regardless of the CME speed type or the X-ray flare class. Figure 8 shows the average values of the peak intensities for Classes 0 to 4 for all events regardless of the associated CME speed or X-ray flare (black symbols; i.e., the values listed in the last column of Table 3) and for those events associated with CMEs of speeds >1000 km $s^{-1}$ (gray symbols; i.e., adding the events associated with CME speed types O and R). Figure 8 shows that the events observed inside an ICME (Class 3) have, on average, higher peak intensities than the other classes of events, followed by events in Class 4 (i.e., observed when an ICME is beyond the observer). Differences in the averaged peak intensities among the different classes of events are more evident when the whole group of events regardless of the CME speed is considered (black symbols in Figure 8). Among the different energies and species analyzed, 175–315 keV electrons and low-energy protons show differences more accentuated among the averaged peak intensities in the different classes of events, whereas the differences are less apparent for P5 40–80 MeV proton intensities.

Figure 8 also shows that, when statistics are significant, the events with intervening ICMEs (i.e., Class 1 events) tend to have, on average and over the ensemble of events, low intensities, especially for 9–15 and 15–40 MeV protons. For 40–80 MeV protons the number of Class 1 events is very limited, whereas for 175–315 keV electrons, there is no significant difference between average peak intensities of Class 0 and Class 1 events. The difference between the average peak intensities of Class 0 and Class 1 events in the P3, P4, and DE4 energy channels is smaller that the difference between the average peak intensity of either Class 3 or Class 4 events and that of the Class 0 events. When considering only events associated with >1000 km $s^{-1}$ CMEs (gray symbols), the number of Class 1 events is not statistically significant to establish a firm comparison with the other classes.

As described in section 2.2, the use of near-Earth in situ ICME observations to determine the presence of an ICME between the Sun and Earth affecting the transport of SEPs may be limited. Therefore, we study here the dependence of the peak intensity for those SEP events associated with or without a preceding LASCO CME fulfilling the criteria described in section 2.2. Figure 9 shows, with the same format as Figure 5, the peak intensity of the SEP events as a function of the primary CME speed. The panels on the left column of Figure 9 consider all events classified in column 15 of Table 1 as P (red open circles), NP* (green solid symbols), and NP (blue crosses). In order to exclude the effects that preceding ICMEs located at or beyond 1 AU may have

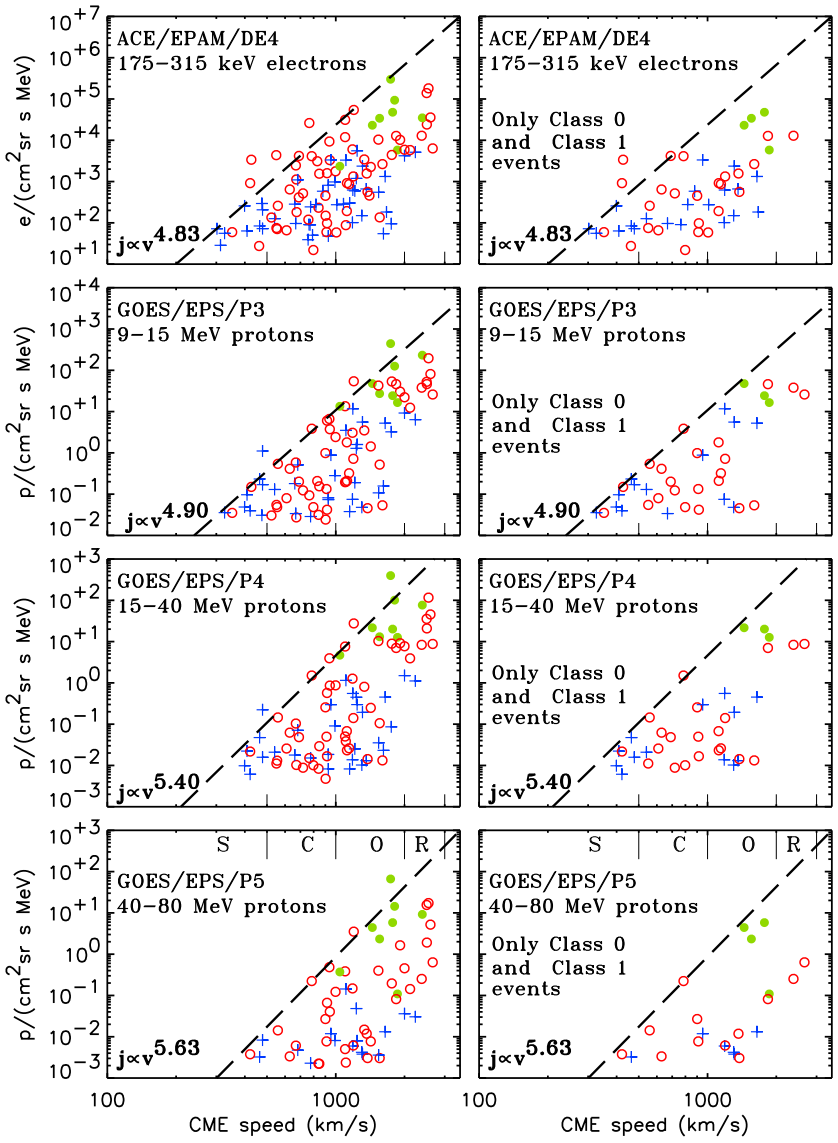


**Figure 9.** SEP peak intensities versus sky-plane speed of the associated CMEs, distinguishing events with a preceding CME (open red symbols for events indicated by P in Column 15 of Table 1), and without a preceding CME (blue crosses for events indicated NP in Column 15 of Table 1 and green solid circles for events indicated NP* in Column 15 of Table 1). Left panels contain all events associated with flares on the frontside of the Sun and regardless of their class based on the in situ observation of ICMEs. Right panels contain only Class 0 and Class 1 events.

on the SEP peak intensities, we have considered, in Figure 9 (right), only those events that were classified as Class 0 or Class 1 according to the criteria described in section 2.1 (i.e., we have excluded events in Classes 2, 3, 4, and 5).

When considering all the possible classes of events (Figure 9, left), we see that there is a considerable overlap between the peak intensities of P and NP events; however, for the most intense SEP events, there is a preponderance of P and NP* events over the NP events. In spite of the overlap, for a given CME speed, Figure 9 (left) shows that the events without any preceding CME (blue crosses) tend to have lower intensities than the events with a preceding CME (red open and green solid symbols), corroborating the results of *Gopalswamy et al.* [2004]. We also see that most of the events associated with fast CMEs (type R) were preceded by a CME from the same source region because fast CMEs tend to occur in a sequence [e.g., *Ruzmaikin et al.*, 2011]. When considering only those events in Class 0 and 1 (Figure 9, right), the distributions become less populated with a deficit of intense events. There is also a significant deficit of NP events (blue crosses) in the proton energy channels associated with C-type speed CMEs. With the exception of six P and NP* events

Journal of Geophysical Research: Space Physics

10.1002/2014JA019771

**Table 4.** Peak Intensity Averages for SEP Events Generated in the Frontside of the Sun with Either the Presence (P) or Absence (NP) of a Preceding > 60° LASCO CME From the Same Source Region and Within 24 h of the Primary CME[a]

| Energy Channel | | CME | | | | Flare | | | All Events[b] |
|---|---|---|---|---|---|---|---|---|---|
| | | S | C | O | R | C | M | X | |
| DE4 NP[c] | All Classes | 9.60E1 (9) | 2.32E2 (15) | 1.63E3 (25) | 1.34E4 (2) | 1.49E2 (18) | 9.05E2 (24) | 3.43E3 (9) | 6.05E2 (51) |
| | *Only Class 0 and Class 1* | *8.58E1 (6)* | *2.90E2 (6)* | *1.57E3 (12)* | *– (0)* | *1.93E2 (12)* | *8.18E2 (9)* | *4.91E3 (3)* | *4.97E2 (24)* |
| DE4 NP (excluding NP*)[d] | All Classes | 9.60E1 (9) | 2.32E2 (15) | 5.37E2 (18) | 5.13E3 (1) | 1.49E2 (18) | 5.38E2 (21) | 2.69E2 (4) | 2.94E2 (43) |
| | *Only Class 0 and Class 1* | *8.58E1 (6)* | *2.90E2 (6)* | *4.21E2 (8)* | *– (0)* | *1.93E2 (12)* | *3.83E2 (7)* | *7.23E1 (1)* | *2.34E2 (20)* |
| DE4 P | All Classes | 2.67E2 (4) | 5.73E2 (28) | 2.02E3 (22) | 2.70E4 (7) | 1.83E2 (5) | 6.92E2 (31) | 5.45E3 (23) | 1.34E3 (61) |
| | *Only Class 0 and Class 1* | *2.67E2 (4)* | *2.64E2 (11)* | *8.92E2 (9)* | *1.29E4 (1)* | *1.42E2 (2)* | *4.32E2 (14)* | *7.68E2 (8)* | *4.79E2 (25)* |
| P3 NP[c] | All Classes | 9.87E−2 (8) | 1.37E−1 (9) | 3.02E0 (21) | 3.85E1 (2) | 1.38E−1 (13) | 1.78E0 (18) | 2.87E0 (9) | 8.64E−1 (40) |
| | *Only Class 0 and Class 1* | *8.01E−2 (6)* | *1.57E−1 (3)* | *3.52E0 (8)* | *– (0)* | *1.65E−1 (10)* | *3.27E0 (5)* | *2.03E0 (2)* | *5.35E−1 (17)* |
| P3 NP (excluding NP*)[d] | All Classes | 9.87E−2 (8) | 1.37E−1 (9) | 7.82E−1 (14) | 6.36E1 (1) | 1.38E−1 (13) | 8.52E−1 (15) | 8.48E−2 (4) | 3.05E−1 (32) |
| | *Only Class 0 and Class 1* | *8.01E−2 (6)* | *1.57E−1 (3)* | *1.04E0 (5)* | *– (0)* | *1.65E−1 (10)* | *7.80E−1 (3)* | *1.70E−1 (1)* | *2.31E−1 (14)* |
| P3 P | All Classes | 7.27E−2 (2) | 2.30E−1 (24) | 2.21E0 (19) | 4.66E1 (7) | 1.74E−1 (3) | 2.77E−1 (27) | 7.92E0 (21) | 1.03E0 (52) |
| | *Only Class 0 and Class 1* | *7.27E−2 (2)* | *2.04E−1 (11)* | *5.17E−1 (7)* | *3.14E1 (2)* | *1.01E−1 (2)* | *3.66E−1 (12)* | *7.81E−1 (7)* | *3.94E−1 (22)* |
| P4 NP[c] | All Classes | 2.46E−2 (6) | 3.36E−2 (8) | 5.69E−1 (22) | 9.23E0 (2) | 2.91E−2 (10) | 3.06E−1 (19) | 1.06E0 (9) | 2.21E−1 (38) |
| | *Only Class 0 and Class 1* | *1.59E−2 (5)* | *7.88E−2 (2)* | *4.29E−1 (9)* | *– (0)* | *3.47E−2 (8)* | *4.08eE−1 (6)* | *5.63E−1 (2)* | *1.24E−1 (16)* |
| P4 NP (excluding NP*)[d] | All Classes | 2.46E−2 (6) | 3.36E−2 (8) | 9.23E−2 (15) | 1.11E0 (1) | 2.91E−2 (10) | 1.19E−1 (16) | 2.05E−2 (4) | 5.88E−2 (30) |
| | *Only Class 0 and Class 1* | *1.59E−2 (5)* | *7.88E−2 (2)* | *6.68E−2 (6)* | *– (0)* | *3.47E−2 (4)* | *6.40E−2 (4)* | *1.58E−2 (1)* | *3.94E−2 (13)* |
| P4 P | All Classes | 2.17E−2 (1) | 6.04E−2 (22) | 4.68E−1 (19) | 1.96E1 (7) | 2.92E−2 (3) | 6.54E−2 (25) | 3.38E0 (20) | 2.99E−1 (49) |
| | *Only Class 0 and Class 1* | *2.17E−2 (1)* | *4.87E−2 (11)* | *6.93E−2 (7)* | *8.56E0 (2)* | *1.53E−2 (2)* | *7.82E−2 (12)* | *2.72E−1 (6)* | *8.62E−2 (21)* |
| P5 NP[c] | All Classes | 5.19E−3 (2) | 5.68E−3 (4) | 1.40E−1 (16) | 5.30E−1 (2) | 5.72E−3 (4) | 5.01E−2 (13) | 5.34E−1 (7) | 6.95E−2 (24) |
| | *Only Class 0 and Class 1* | *3.24E−3 (1)* | *1.18E−2 (1)* | *9.76E−2 (8)* | *– (0)* | *5.72E−3 (4)* | *6.83E−2 (4)* | *3.69E0 (2)* | *5.62E−2 (10)* |
| P5 NP (excluding NP*)[d] | All Classes | 5.19E−3 (2) | 5.68E−3 (4) | 1.28E−2 (9) | 3.05E−2 (1) | 5.72E−3 (4) | 1.44E−2 (10) | 4.31E−3 (2) | 9.84E−3 (16) |
| | *Only Class 0 and Class 1* | *3.24E−3 (1)* | *1.18E−2 (1)* | *5.95E−3 (4)* | *– (0)* | *5.72E−3 (4)* | *6.71E−3 (2)* | *– (0)* | *6.03E−3 (6)* |
| P5 P | All Classes | 3.77E−3 (1) | 2.17E−2 (12) | 4.83E−2 (16) | 1.80E0 (7) | 3.04E−3 (1) | 1.09E−2 (15) | 3.27E−1 (20) | 6.96E−2 (36) |
| | *Only Class 0 and Class 1* | *3.77E−3 (1)* | *1.86E−2 (5)* | *1.16E−2 (4)* | *4.00E−1 (2)* | *– (0)* | *1.50E−2 (6)* | *3.60E−2 (6)* | *2.32E−2 (12)* |

[a] Averages computed using the logarithm of the peak intensities in each CME speed type (S, C, O, and R) and each soft X-ray flare class (C, M, and X) for the energy channels DE4 (175–315 keV electrons), P3 (9–15 MeV protons), P4 (15–40 MeV protons), and P5 (40–80 MeV protons). The first row in each event group considers all events regardless of their Class based on the in situ observation of ICMEs, whereas the second raw (in italics) considers only events of Class 0 and Class 1.

[b] Regardless of flare or CME association.

[c] All events listed as NP in Column 15 of Table 1.

[d] All events listed as NP in Column 15 of Table 1 but excluding those events listed as NP*.

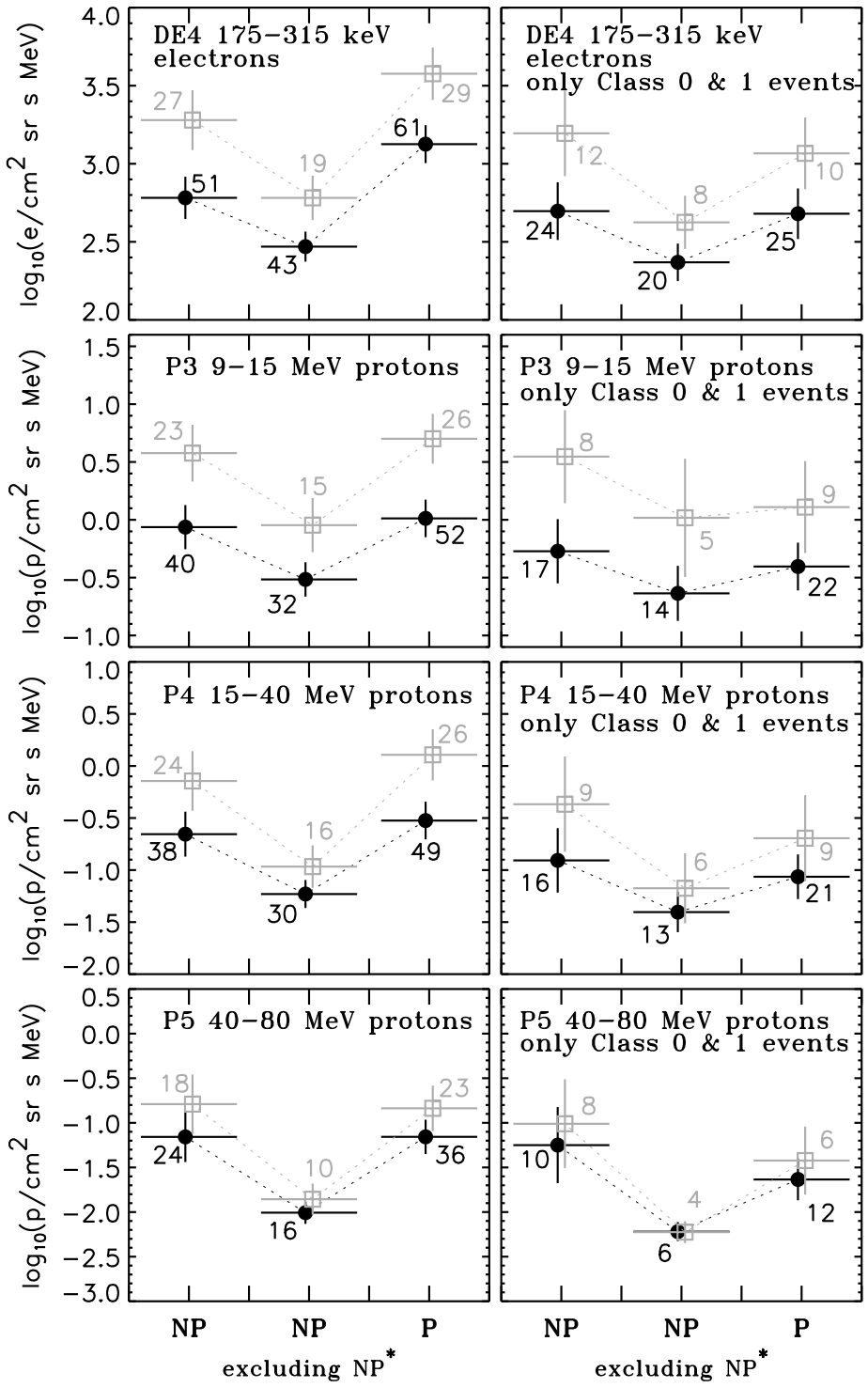


**Figure 10.** Average values of the peak intensities of the prompt component of the SEP events (black symbols) regardless of the associated CME speed or X-ray flare class and (gray symbols) associated with CMEs of speed >1000 km $s^{-1}$, from left to right, classified as NP in column 15 of Table 1, classified as NP but excluding the events with NP*, and the events classified as P, for the energy channels, from top to bottom, DE4, P3, P4, and P5. Left panels contain all events associated with flares on the frontside of the Sun and regardless of their class based on the in situ observation of ICMEs. Right panels contain only Class 0 and Class 1 events. The numbers indicate the number of events in each group NP, pure NP, and P. The vertical bars indicate the standard errors obtained from the average of the logarithms of the peak intensities.

in the top right corner of Figure 9 (right) (associated with the fastest CMEs) and the C-type CME speed bin (where P events are more abundant), the preponderance of P events (red open circles) over NP events (blue crosses) at high intensities is not so clear as when we consider all classes of events. Note that we have not distinguished NP* events among the less intense NP events, and some of the blue crosses in Figure 9 may become green solid symbols.

We have listed in Table 4 the averages of the peak intensities for each energy channel, in each event group (P, NP, and NP excluding the NP* events), for each CME speed type and for each soft X-ray flare class. We have distinguished the averages obtained when considering all events regardless of their class (i.e., the events shown in Figure 9 (left) and listed in the first row of each event group in Table 4) from the averages obtained when considering only Class 0 and Class 1 events (i.e., the events shown in Figure 9 (right) and listed in the second row of each group in Table 4 using italic font). Figure 10 (left column) shows, with the same format as Figure 8, the averages of the SEP peak intensities for those events plotted in Figure 9 (left column), for each energy channel (from top to bottom) and, from left to right, the events classified as NP, classified as NP but excluding NP*, and classified as P (from left to right). The distinction between the averaged peak intensities of the P and NP events is only obtained when NP* events are excluded. Figure 10 (right column) shows the same averages but considering only Class 0 and Class 1 SEP events (i.e., the events plotted in Figure 9, right). Although the average peak intensity of P events is larger than that of the pure NP events (i.e., events NP excluding events NP*), the distinction is less clear than when all the events (regardless of their class) are considered. Note that we have not distinguished, among the NP events, those that can be classified as NP* for the whole range of intensities, which may modify this result. Table 4 also shows that the distinction between average peak intensities in different groups is more ambiguous when comparing events associated with similar X-ray flares rather than similar CME speed.

## 5. Conclusions

We have analyzed the peak intensity measured in the prompt component of western SEP events observed throughout solar cycle 23 near Earth. With a considerable degree of scatter, there is a trend for intense SEP events to be associated with fast CMEs. However, rather than suggesting possible correlations between the logarithm of the SEP peak intensities and the logarithm of the CME speeds [e.g., *Gopalswamy et al.*, 2004; *Park et al.*, 2012; *Miteva et al.*, 2013], we propose the use of triangular distributions (Figure 5) that provide, for a given CME speed, an upper limit of the peak intensity measured in the prompt component of the SEP events. When we include all SEP events regardless of their longitudinal solar origin (not shown here), the triangular distributions maintain their basic shape, with the only effect of being more populated than those shown in Figure 5. The distributions of the prompt component peak intensities versus the soft X-ray peak flux of the associated flares do not follow clear log-log correlations (Figure 6). Correlations between SEP peak intensities and soft X-ray flare classes only improve when intense flares, western flares, long-duration flares or average values in certain flare sizes, and SEP intensity bins are used [e.g., *Park et al.*, 2010; *Wang*, 2006; *Belov et al.*, 2005].

We have classified the SEP events according to the presence or absence of ICMEs in the IP medium at the time when the peak intensity of the prompt component of the SEP event is observed. In situ observations of ICMEs near Earth have been used to determine the presence and location of prior ICMEs. We have divided the SEP events into the following categories: (0) the event is observed under undisturbed nominal solar wind conditions (i.e., in absence of ICMEs); (1) the event occurs when an ICME is located between Earth and Sun; (2) the peak intensity of the prompt component of the SEP event is observed in the sheath region of a preceding ICME; (3) the peak intensity of the prompt component of the SEP event is observed within an ICME; (4) the peak intensity of the prompt component of the SEP event is observed when an ICME is located beyond Earth; and (5) multiple scenarios with ICMEs located beyond the observer and between the Sun and Earth. The statistical analysis of SEP peak intensities in the prompt component of the SEP events shows that, over the ensemble of events, the highest peak intensities, on average, are observed when the spacecraft is inside an ICME followed by the events observed when an ICME is beyond Earth. By contrast, the few events observed when an Earth-directed ICME is located between the Sun and Earth show, on average, lower peak intensities than those of the events observed under undisturbed solar wind conditions, especially for 9–15 and 15–40 MeV proton intensities. The difference is not significant for 175–315 keV electron peak intensities (Figures 4 and 8).

A similar study was performed by *Miteva et al.* [2013] who considered SEP events in solar cycle 23 associated with M class or X class solar flares occurring on the western hemisphere of the Sun (W0°–W90°). Rather than considering the IP conditions when the peak intensity in the prompt component of the event was observed, *Miteva et al.* [2013] classified the events according to the IP conditions at the time of the onset of the event. *Miteva et al.* [2013] categorized a total of 104 SEP events as (1) observed within an ICME, (2) observed in the standard solar wind when the onset of the SEP event occurred at least 1 day after the end of a previous ICME at Earth and at least 1 day before the start of the next ICME, and (3) the remaining events with uncertain magnetic field configurations including the vicinity of shocks, sheath regions, or disturbed field lines behind ICMEs. Location of ICMEs was based on in situ plasma and magnetic field observations. The different criteria used here together with the use of particle data with different time resolution and different time intervals to determine the presence or absence of ICMEs lead to slight discrepancies among the class assigned to each event. However, most of the events that *Miteva et al.* [2013] classified as observed within an ICME are in our Class 3. Most of the events that *Miteva et al.* [2013] classified as observed in the standard solar wind are in our Class 0 for the common energy channels analyzed in both works. Events that *Miteva et al.* [2013] classified as observed in the vicinity of ICMEs are mostly divided among our Classes 2–4. *Miteva et al.* [2013] stated that the differences in the peak intensity distributions of those events observed within an ICME and of the events observed in the standard solar wind were not statistically significant, although there was a preponderance for higher peak intensities in the events observed inside an ICME (see their Figure 1). The results presented in our work, including the distinction between events observed before or after the passage of an ICME and longer time intervals to determine the presence of ICMEs, show that the peak intensity distribution of events observed within an ICME differ from those observed in undisturbed solar wind (Figure 4). The events observed within an ICME have, on average, higher intensities than those events observed outside of ICMEs (Figures 4 and 8 and Table 3). The events observed after the passage of an ICME are typically associated with fast CMEs (Figure 7), and hence, their averaged peak intensities are higher than those of the events observed when the passage of preceding ICMEs occurs after the onset the SEP event (i.e., higher than Class 1 events).

The fact that SEP events observed within ICMEs or after the passage of an ICME have, on average, higher peak intensities than events observed in undisturbed solar wind (Figure 8) may be interpreted as follows. Both (1) the magnetic topology of the ICMEs and (2) the interplanetary perturbations associated with the ICMEs located beyond 1 AU provide the magnetic structures necessary to reflect SEPs back toward the observer leading to the observation of elevated SEP intensities at 1 AU. The fact that fast CMEs tend to occur in series [*Ruzmaikin et al.*, 2011] implies also that the most intense SEP events usually occur under the presence of ICME structures in the IP medium which may modify the nominal transport of SEPs. For example, *Miteva et al.* [2013] found that the fraction of SEP events detected within an ICME increases with the associated flare size, indicating that the more energetic the solar event associated with the origin of the SEP event, the greater the likelihood to detect the SEP event within or in the vicinity of an ICME. Both the frequent association with fast CMEs and the possible effect that preceding ICMEs have on the transport of SEPs contribute to the higher intensities observed in events of Classes 3 and 4.

On the other hand, one may also expect that when a SEP event occurs with a preceding ICME located between the Sun and the observer, the effect that this intervening structure has on the SEP transport may lead to an attenuation of the observed SEP intensities with respect to the intensities observed in the case of an event occurring in an undisturbed solar wind. Our results based on in situ observation of ICMEs show that (1) the number of events with ICME located between the Sun and Earth was low and (2) the average peak intensity of the Class 1 events is slightly lower than that of the other Classes for 9–15 and 15–40 MeV protons, but for 175–315 keV electrons does not differ significantly from those events observed under undisturbed solar wind conditions (cf. Figures 4 and 8). The fact that ICMEs located beyond Earth have a greater impact on the observed SEP peak intensities than the ICMEs located between the Sun and Earth may result from the fact that particles propagating close to the Sun tend to focus along the magnetic field. The diverging magnetic field close to the Sun focus the particles along the magnetic field with small pitch angles which make them able to easily overcome magnetic field enhancements. At larger heliocentric distances (particularly when the magnetic field begins to fall off as $1/r$ where $r$ is the heliocentric distance), scattering and mirroring processes are more efficient reflecting particles back to 1 AU. Hence, ICMEs located beyond 1 AU have a larger effect on the transport of SEPs than ICMEs close to the Sun.

The limitations of using in situ observations of ICMEs to determine the presence of an intervening ICME affecting the transport of SEPs led us to use LASCO observations to determine the presence of an ICME launched from the same source region as the CME origin of the SEP event and within 24 h of the primary CME. This is the same criteria used by *Gopalswamy et al.* [2004] to conclude that the preconditioning of the medium by the preceding CME favors the efficient acceleration of particles by the shock driven by the primary CME, and hence the higher peak intensities in P events. When considering all events regardless of their class, we duplicate the results of *Gopalswamy et al.* [2004] but now including events with lower intensities than those considered by *Gopalswamy et al.* [2004] (Figures 9 (left) and 10 (left)). However, when we exclude those events affected by the presence of a preceding ICME at or beyond 1 AU, the difference between the average peak intensities of events P and pure NP (i.e., NP events excluding NP*) becomes smaller (Figures 9 (right) and 10 (right)). Therefore, we conclude that the preconditioning of the medium produced by a preceding CME may lead to an efficient acceleration of particles, but other factors such as those produced by interplanetary structures by preceding ICMEs located at or beyond the observer need to be considered when studying the variability of the measured SEP intensities.

**Acknowledgments**

We acknowledge the use of the CDAW CME catalog generated and maintained at the CDAW Data Center by NASA and The Catholic University of America in cooperation with the Naval Research Laboratory. We acknowledge the use of the near-Earth interplanetary coronal mass ejection list compiled by I.G. Richardson and H.V. Cane. SOHO is a project of international cooperation between ESA and NASA. We acknowledge the support from NASA under grants NNX09AG30G, NNX11A083G, the ACE grant NNX10AT75G, and the Solar Probe Plus NASA contract NNN06AA01C. A.K. acknowledges the support received from the Summer Internship Program of JHU/APL. D.L. wants to acknowledge the International Space Science Institute (ISSI) working team "Exploration of the inner heliosphere—What we have learned from Helios and what we want to study with Solar Orbiter" for stimulating discussions and the support received from ISSI. We thank both referees for helpful suggestions.

Yuming Wang thanks Ian G. Richardson and Stephen Kahler for their assistance in evaluating this paper.

## References

Belov, A., H. Garcia, V. Kurt, H. Mavromichalaki, and M. Gerontidou (2005), Proton enhancements and their relation to X-ray flares during the last three solar cycles, *Sol. Phys.*, *229*, 135–159.

Cane, H. V., and D. Lario (2006), An introduction to CMEs and energetic particles, *Space Sci. Rev.*, *123*, 45–56.

Cane, H. V., and I. G. Richardson (2003), Interplanetary coronal mass ejections in the near-Earth solar wind during 1996–2002, *J. Geophys. Res.*, *108*, 1156, doi:10.1029/2002JA009817.

Cane, H. V., D. V. Reames, and T. T. von Rosenvinge (1988), The role of interplanetary shocks in the longitude distribution of solar energetic particles, *J. Geophys. Res.*, *93*, 9555–9567, doi:10.1029/JA093iA09p09555.

Cane, H. V., I. G. Richardson, and T. T. von Rosenvinge (2010), A study of solar energetic particle events of 1997–2006: Their composition and associations, *J. Geophys. Res.*, *115*, A08101, doi:10.1029/2009JA014848.

Cliver, E. W., A. G. Ling, A. Belov, and S. Yashiro (2012), Size distributions of solar flares and solar energetic particle events, *Astrophys. J.*, *756*(2), L29, doi:10.1088/2041-8205/756/2/L29.

Ding, L., Y. Jiang, L. Zhao, and G. Li (2013), The "twin-CME" scenario and large solar energetic particle events in solar cycle 23, *Astrophys. J.*, *763*, 30, doi:10.1088/0004-637X/763/1/30.

Evans, R. M., A. A. Pulkkinen, Y. Zheng, M. Leila Mays, A. Taktakishvili, M. M. Kuznetsova, and M. Hesse (2013), The SCORE scale: A coronal mass ejection typification system based on speed, *Space Weather*, *11*, 333–334, doi:10.1002/swe.20058.

Garcia, H. A. (2004), Forecasting methods for occurrence and magnitude of proton storms with solar soft X-rays, *Space Weather*, *2*, S02002, doi:10.1029/2003SW000001.

Gold, R. E., S. M. Krimigis, S. E. Hawkins III, D. K. Haggerty, D. A. Lohr, E. Fiore, T. P. Arm-strong, G. Holland, and L. J. Lanzerotti (1998), Electron, proton, and alpha monitor on the Advanced Composition Explorer spacecraft, *Space Sci. Rev.*, *86*, 541–562, doi:10.1023/A:1005088115759.

Gopalswamy, N. (2012), Factors affecting the intensity of solar energetic particle events, in *Physics of the Heliosphere: A 10 Year Retrospective*, vol. 1436, pp. 247–252, 10th Annual International Astrophysics Conference (AIAC), Maui, Haw., Am. Inst. Phys., Melville, N. Y.

Gopalswamy, N., S. Yashiro, A. Lara, M. L. Kaiser, B. J. Thompson, P. T. Gallagher, and R. A. Howard (2003), Large solar energetic particle events of cycle 23: A global view, *Geophys. Res. Lett.*, *30*(12), 8015, doi:10.1029/2002GL016435.

Gopalswamy, N., S. Yashiro, S. Krucker, G. Stenborg, and R. A. Howard (2004), Intensity variation of large solar energetic particle events associated with coronal mass ejections, *J. Geophys. Res.*, *109*, A12105, doi:10.1029/2004JA010602.

Gopalswamy, N., S. Yashiro, S. Akiyama, P. Mäkelä, H. Xie, M. L. Kaiser, R. A. Howard, and J. L. Bougeret (2008a), Coronal mass ejections, type II radio bursts, and solar energetic particle events in the SOHO era, *Ann. Geophys.*, *21*, 3033–3047.

Gopalswamy, N., S. Yashiro, H. Xie, S. Akiyama, E. Aguilar-Rodriguez, M. L. Kaiser, R. A. Howard, and J.-L. Bougeret (2008b), Radio-quiet fast and wide coronal mass ejections, *Astrophys. J.*, *674*, 560–569, doi:10.1086/524765.

Hudson, P. D. (1965), Reflection of charged particles by plasma shocks, *Mon. Not. R. Astron. Soc.*, *131*, 23–49.

Hundhausen, A. J. (1972), *Coronal Expansion and Solar Wind*, Phys. Chem. Space, vol. 5, Springer-Verlag, Berlin Heidelberg, New York.

Jiggens, P. T. A., and S. B. Gabriel (2009), Time distributions of solar energetic particle events: Are SEPEs really random?, *J. Geophys. Res.*, *114*, A10105, doi:10.1029/2000JA014291.

Kahler, S. W. (2001), The correlation between solar energetic particle peak intensities and speeds of coronal mass ejections: Effects of ambient particle intensities and energy spectra, *J. Geophys. Res.*, *106*, 20,947–20,955, doi:10.1029/2000JA002231.

Kahler, S. W., and D. V. Reames (2003), Solar energetic particle production by coronal mass ejection-driven shocks in solar fast-wind regions, *Astrophys. J.*, *584*(2), 1063–1070.

Kahler, S. W., J. T. Burkepile, and D. V. Reames (1999), Coronal/interplanetary factors contributing to the intensities of $E > 20$ MeV gradual solar energetic particle events, in *Proceedings of the 26th International Cosmic Ray Conference*, vol. 6, edited by D. Kieda, M. Salamon, and B. Dingus, pp. 248–251, Int. Union of Pure and Appl. Phys. (IUPAP), Utah.

Kahler, S. W., S. Akiyama, and N. Gopalswamy (2012), Deflections of fast coronal mass ejections and the properties of associated solar energetic particle events, *Astrophys. J.*, *754*, 100, doi:10.1088/0004-637X/754/2/100.

Kahler, S. W., C. N. Arge, S. Akiyama, and N. Gopalswamy (2014), Do solar coronal holes affect the properties of solar energetic particle events?, *Sol. Phys.*, *289*, 657–673, doi:10.1007/s11207-013-0427-0.

Kallenrode, M.-B. (2001), The influence of magnetic clouds on the propagation of energetic charged particles in interplanetary space, *Proc. 27th Int. Cosmic Ray Conf.*, pp. 3273–3276, Hamburg, Germany.

Kallenrode, M.-B. (2002), Magnetic clouds and interplanetary particle transport: A numerical model, *J. Atmos. Sol. Terr. Phys.*, *64*(18), 1973–1978, doi:10.1016/S1364-6826(02)00185-5.

Kallenrode, M.-B., and E. W. Cliver (2001), Rogue SEP events: Observational aspects, *Proc. 27th Int. Cosmic Ray Conf.*, pp. 3314–3317, Hamburg, Germany.

Lario, D. (2006), Radial and longitudinal variations of the energetic particle response to ICMEs, *Solar Eruptions and Energetic Particles, Geophys. Monogr. Ser.*, vol. 165, pp. 309–319, AGU, Washington, D. C., doi:10.1029/165GM29.

Lario, D., M.-B. Kallenrode, R. B. Decker, E. C. Roelof, S. M. Krimigis, A. Aran, and B. Sanahuja (2006), Radial and longitudinal dependence of solar 4–13 MeV and 27–37 MeV proton peak intensities and fluences: Helios and IMP-8 observations, *Astrophys. J.*, *653*(2), 1531–1544.

Lario, D., R. B. Decker, and A. Aran (2008), Solar energetic particle intensities above the streaming limit, in *Particle Acceleration and Transport in the Heliosphere and Beyond: 7th Annual International Astrophysics Conference*, vol. 1039, pp. 156–161, AIP Conf. Proc.

Lario, D., A. Aran, R. Gómez-Herrero, N. Dresing, B. Heber, G. C. Ho, R. B. Decker, and E. C. Roelof (2013), Longitudinal and radial dependence of solar energetic particle peak intensities: Stereo, ace, soho, goes, and messenger observations, *Astrophys. J.*, *767*(1), 41, doi:10.1088/0004-637X/767/1/41.

Li, G., R. Moore, R. A. Mewaldt, L. Zhao, and A. W. Labrador (2012), A twin-CME scenario for ground level enhancement events, *Space Sci. Rev.*, *171*, 141–160, doi:10.1007/s11214-011-9823-7.

Miteva, R., K.-L. Klein, O. Malandraki, and G. Dorrian (2013), Solar energetic particle events in the 23rd solar cycle: Interplanetary magnetic field configuration and statistical relationship with flares and CMEs, *Sol. Phys.*, *282*, 579–613.

Onsager, T., R. Grubb, J. Kunches, L. Matheson, D. Speich, R. W. Zwickl, and H. Sauer (1996), Operational uses of the GOES energetic particle detectors, in *GOES-8 and Beyond*, vol. 2812, edited by E. R. Washwell, pp. 281–290, Proc. SPIE, Bellingham, Wash.

Park, J., Y.-J. Moon, D. H. Lee, and S. Youn (2010), Dependence of solar proton events on their associated activities: Flare parameters, *J. Geophys. Res.*, *115*, A10105, doi:10.1029/2010JA015330.

Park, J., Y.-J. Moon, and N. Gopalswamy (2012), Dependence of solar proton events on their associated activities: Coronal mass ejection parameters, *J. Geophys. Res.*, *117*, A08108, doi:10.1029/2011JA017477.

Reames, D. V. (2000), Particle acceleration by CME-driven shock waves, in *26th Int. Cosmic Ray Conf.: ICRC XXVI, Invited, Rapporteur, and Highlight Papers*, vol. 516, pp. 289–300, AIP Conf. Proc.

Reames, D. V., and C. K. Ng (1998), Streaming-limited intensities of solar energetic particles, *Astrophys. J.*, *504*, 1002–1005, doi:10.1086/306124.

Richardson, I. G., and H. V. Cane (1996), Particle flows observed in ejecta during solar event onsets and their implication for the magnetic field topology, *J. Geophys. Res.*, *101*, 27,521–27,532, doi:10.1029/96JA02643.

Richardson, I. G., and H. V. Cane (2010), Near-Earth interplanetary coronal mass ejections during solar cycle 23 (1996–2009): Catalog and summary of properties, *Sol. Phys.*, *264*, 189–237, doi:10.1007/s11207-010-9568-6.

Ruzmaikin, A., J. Feynman, and S. A. Stoev (2011), Distribution and clustering of fast coronal mass ejections, *J. Geophys. Res.*, *116*, A04220, doi:10.1029/2010JA016247.

Sauer, H. H. (1993), GOES observations of energetic protons to $E > 685$ MeV: Description and data comparison, *Proc. 23rd Int. Cosmic Ray Conf.*, 250–253.

Vandas, M., S. Fischer, A. Geranios, M. Dryer, Z. Smith, and T. Detman (1996), Magnetic traps in the interplanetary medium associated with magnetic clouds, *J. Geophys. Res.*, *101*, 21,589–21,596, doi:10.1029/96JA01640.

Wang, R. (2006), Statistical characteristics of solar energetic proton events from January 1997 to June 2005, *Astroparticle Phys.*, *26*, 202–208, doi:10.1016/j.astropartphys.2006.06.003.

Yashiro, S., N. Gopalswamy, G. Michalek, O. C. St. Cyr, S. P. Plunkett, N. B. Rich, and R. A. Howard (2004), A catalog of white light coronal mass ejections observed by the SOHO spacecraft, *J. Geophys. Res.*, *109*, A07105, doi:10.1029/2003JA010282.